Magnetic Susceptibility of Halifax Formation Slates at the Halifax International Airport: Correlation with Potential for Acid Drainage

Kerry Knee

Submitted in Partial Fulfiiment of the Requirements
for the Degree of Bachelor of Science, Honours
Department of Earth Sciences
Dalhousie University, Halifax, Nova Scotia
March 1995

Distribution License

DalSpace requires agreement to this non-exclusive distribution license before your item can appear on DalSpace.

NON-EXCLUSIVE DISTRIBUTION LICENSE

You (the author(s) or copyright owner) grant to Dalhousie University the non-exclusive right to reproduce and distribute your submission worldwide in any medium.

You agree that Dalhousie University may, without changing the content, reformat the submission for the purpose of preservation.

You also agree that Dalhousie University may keep more than one copy of this submission for purposes of security, back-up and preservation.

You agree that the submission is your original work, and that you have the right to grant the rights contained in this license. You also agree that your submission does not, to the best of your knowledge, infringe upon anyone's copyright.

If the submission contains material for which you do not hold copyright, you agree that you have obtained the unrestricted permission of the copyright owner to grant Dalhousie University the rights required by this license, and that such third-party owned material is clearly identified and acknowledged within the text or content of the submission.

If the submission is based upon work that has been sponsored or supported by an agency or organization other than Dalhousie University, you assert that you have fulfilled any right of review or other obligations required by such contract or agreement.

Dalhousie University will clearly identify your name(s) as the author(s) or owner(s) of the submission, and will not make any alteration to the content of the files that you have submitted.

If you have questions regarding this license please contact the repository manager at dalspace@dal.ca.

Grant the distribution license by signing and dating below.

_____ _____

Name of signatory Date

Dalhousie University

Department of Earth Sciences
Halifax, Nova Scotia
Canada B3H 3J5
(902) 494-2358
FAX (902) 494-6889

DATE May 16,1995

AUTHOR Kerry Knee

TITLE Magnetic Susceptibility of Halifax Formation Slates at the Halifax International Airport: Correlation with Potential for Acid Drainage

Degree BSc Convocation May 23, 1995 Year 1995

Permission is herewith granted to Dalhousie University to circulate and to have copied for non-commercial purposes, at its discretion, the above title upon the request of individuals or institutions.

Abstract

The disruption by excavation or quarrying of sulphide-rich slate units of the Halifax Formation of the Meguma Group of Nova Scotia leads to oxidation of the sulphides and generation of acid drainage. Construction within the area of the Halifax International Airport (HIA) since 1955 has caused the most serious problems. Expensive measures were required to avoid fish kills in rivers draining from the HIA. Previous studies assumed that the mineral responsible for the acid drainage was pyrite (FeS_2) but recent work at Dalhousie University has shown, and this study has confirmed, that the most abundant sulphide in the slates of the HIA is monoclinic pyrrhotite (Fe_7S_8). Monoclinic pyrrhotite is a magnetic mineral. This thesis is a pilot study which measured the magnetic susceptibility of representative rock powders and drill cores as a means of predicting the percentage amount of pyrrhotite in slates from the HIA as an indirect measure of their acid drainage potential. To this purpose, the laboratory conducted magnetic susceptibility measurements of representative rock powders and drill core samples. Reflected light microscopy and microprobe analyses of the same samples was used to determine the mineralogy. As a first approximation, pyrrhotite has a positive correlation with magnetic susceptibility in solid drillcore samples, although the inhomogeneous distribution of sulphides in the rock leads to substantial uncertainty at the scale of the experiment. The correlation is poor in powdered samples stored for several years; however, these results may reflect sampling error or recent oxidation of the sulphides in the vials.

Key words: magnetic susceptibility, sulphide-mineralogy, pyrrhotite, acid drainage, Halifax Formation, Halifax International Airport.

I dedicate this thesis

to my parents,

Don and Dulcie Knee.

Table of Contents

Table of Figures

Table of Tables

Acknowledgements

I wish to thank the following people for making this honours thesis possible: my thesis advisor, Dr. Marcos Zentilli, for his guidance and supervision during the preparation of this thesis; Dr. Ian MacInnis and Dr. Milton Graves for supplying drill core, powdered samples and thin sections; Don Fox, for his continuous input and assistance; Charlie Walls, for his help with the magnetic susceptibility meters; and Robert McKay, for his assistance on the microprobe. I would like to extend a special thanks to our thesis class professor, Dr. Barrie Clarke, for his tireless dedication to all of his students.

CHAPTER 1: INTRODUCTION

1.1 Background, Purpose, and Scope

Much of southern Nova Scotia is underlain by sulphide-rich black slates, primarily concentrated in the Halifax Formation of the Cambro-Ordovician Meguma Group. In their natural state, these slates pose little harm to the environment; however, when disturbed, the sulphide in these slates reacts with water and oxygen to produce abnormally high concentrations of sulphuric acid. The extensive outcrops of these sulphide-rich slates has led to a serious problem of acid generation in Nova Scotia. The bedrock of the Halifax International Airport (HIA) belongs to the Halifax Formation and has been producing acid runoff since construction began in 1955 (Lund 1987).

The amount of acid runoff produced from sulphide-rich slates increases with increasing modal percentages of pyrite or pyrrhotite. Previous studies (Roberts 1986; NSRFC 1985) have assumed the predominant sulphide mineral of the Halifax Formation to be pyrite; however, ongoing studies by MacInnis et al. (1994) have shown that pyrrhotite far exceeds the abundance of pyrite. Unlike pyrite, pyrrhotite is magnetic with the ability to take on induced magnetism, which is a measure of its *magnetic susceptibility*. Therefore, if the abundance of pyrrhotite is directly proportional to the amount of acid drainage produced, and if the abundance of pyrrhotite is directly proportional to magnetic susceptibility, it is probable that magnetic susceptibility could be used as an indicator of the potential production of acid drainage. Therefore, the purpose of this study is to test

the hypothesis that magnetic susceptibility is an accurate predictor of the abundance of pyrrhotite through a pilot study of the mineralogy of the slates at the HIA. This is only a first step towards evaluating the potential value of this physical property as a predictor of acid drainage potential.

The scope of this thesis is restricted to the Halifax Formation slates at the HIA because of its extensive and well-documented history concerning acid drainage from black slates. Study of the mineralogy of the slates is restricted to the iron-sulphide bearing minerals, such as pyrrhotite, pyrite, chalcopyrite, and arsenopyrite.

This study should be considered only as a preliminary assessment of the problem, carried out as a student project between September 1994 and Feburary 1995.

1.2 The Halifax Formation

The Halifax Formation slates belong to the Cambro-Ordovician Meguma Group and comformably overlie the Goldenville Formation metawackes (Schenk 1970). The two formations occur as long alternating bands striking nearly parallel to the southern coast of Nova Scotia (Fig.1.1). The Halifax Formation is a black graphitic slate with minor interbedded greywacke (Horne 1992). The slate exhibits well-developed cleavage (Fig.1.2) and is rich in visible sulphides along these cleavage planes (Figure 1.3). The folding pattern of the Meguma Group results in an exposed area of approximately 125,000 km^2 of this sulphide-rich zone in Nova Scotia.

The transition between the two formations is a significant control for metal concentration. The base of the Halifax Formation, where it borders the Goldenville, is preferentially enriched in Mn, total C, Ba, Pb, Zn, Cu, Mo, W, Au, and S over average

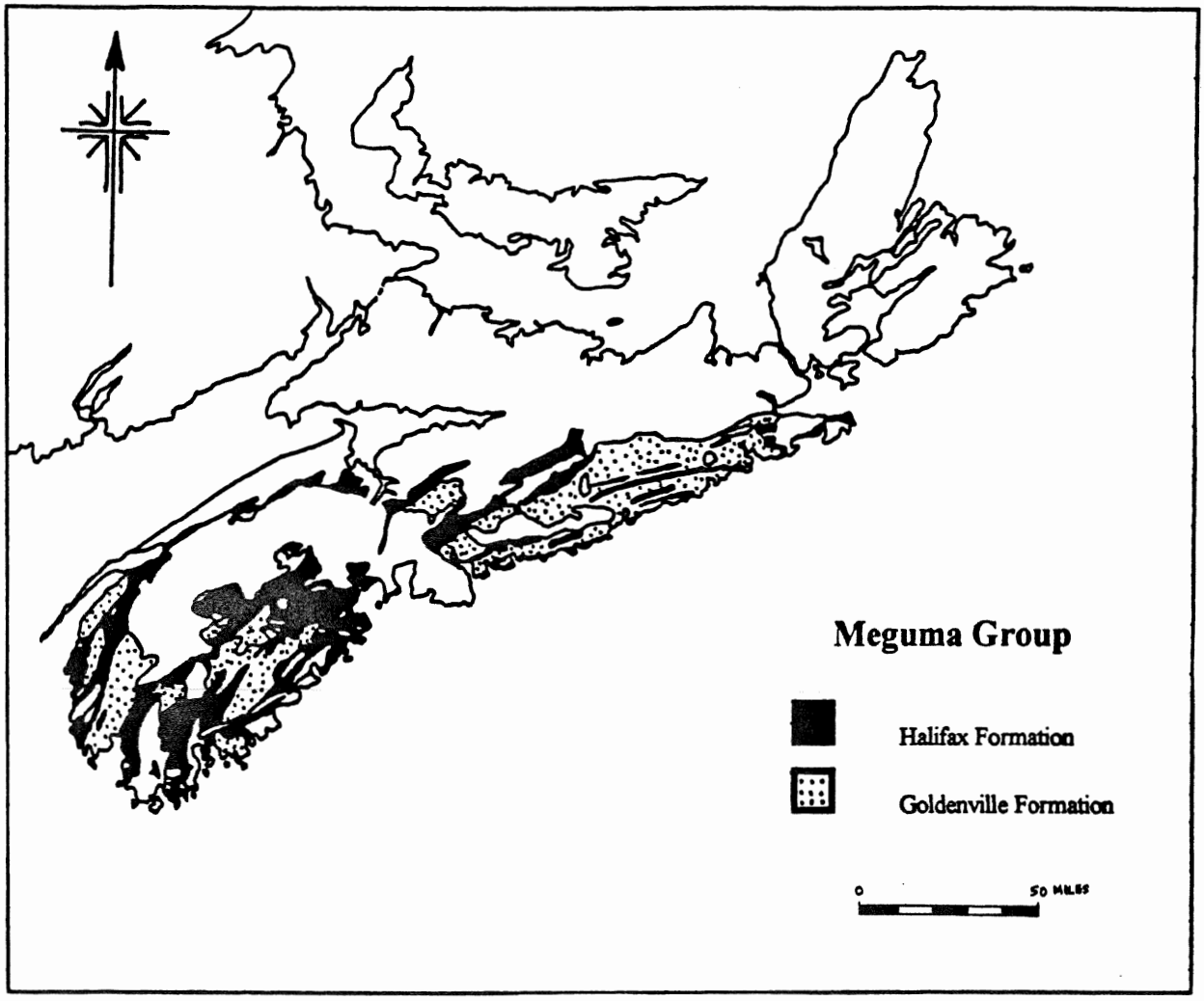

Figure 1.1 Geological map of the Meguma Group in Nova Scotia (N.S. Dept. of Mines, 1979).

? No

Figure 1.2 Halifax Formation slate at the HIA exhibiting well-defined cleavage.

Figure 1.3 Sample # BH-20-2.1 in transmitted light. Pyrrhotite lenses concentrated along cleavage planes (f.o.v. 2.5 cm).

crustal values of the whole formation, and is referred to as the Goldenville-Halifax Transition Zone (GHT) (Graves and Zentilli 1988). This transition zone records a decrease in the supply of dissolved oxygen at the sediment-water interface which resulted in an increase in the amount of sulphides that formed during diagenesis (Waldron and Graves 1987).

1.3 Acid Drainage

Acid drainage is the result of the chemical and/or biological oxidation of metallic sulphides, particularly iron sulphides, creating a highly acidic runoff contaminated with dissolved metallic ions. The following equations simplify the chemical processes involved in acid generation through the oxidation of (1) pyrite (Nordstrom 1982) and (2) pyrrhotite (Nicholson 1994):

$$FeS_2(s) + 15/4\ O_2 + 7/2\ H_2O \rightarrow Fe(OH)_3(s) + 2H_2SO_4(aq) \quad (1.1)$$

$$Fe_{1-x}S + (2-x/2)\ O_2 + x\ H_2O \rightarrow (1-x)\ Fe^{2+} + 3\ Fe^{2+} + SO_4^{2-} + 2xH^+ \quad (1.2)$$

where x can vary from 0.125 to 0.0 depending on the type of pyrrhotite. In general, for the monoclinic variety, x~0.125.

The complete chemical reaction involved in acid generation is a multi-staged process described by the following four reactions (Barnes and Romberger 1968; Baker 1975):

$$FeS_{2\,(s)} + 7/2\ O_2 + H_2O \rightarrow Fe^{2+} + 2SO_4^{2-} + 2H^+ \quad (1.3)$$

$$Fe^{2+} + 1/4\ O_2 + H^+ \rightarrow Fe^{3+} + 1/2H_2O \quad (1.4)$$

$$Fe^{3+} + 3\ H_2O \rightarrow Fe(OH)_{3\,(s)} + 3\ H^+ \quad (1.5)$$

$$FeS_{2\,(s)} + 14\ Fe^{3+} + 8\ H_2O \rightarrow 15\ Fe^{2+} + 2\ SO_4^{2-} + 16\ H^+ \quad (1.6)$$

The stoichiometry of Eq. (1.3) shows that 1 mole of FeS_2 will produce 2 moles of H^+. The Fe^{2+} that is generated can readily oxidize to Fe^{3+} and produce additional H^+ (Eq. (1.4) and (1.5)). Excess Fe^{3+} in solution can contribute to a more rapid rate of oxidation of FeS_2 according to Eq. (1.6). The oxidation of pyrrhotite generates less acid than the oxidation of pyrite; however, pyrrhotite will oxidize at a faster rate than pyrite (MacInnis et al. in progress).

Bedrock beneath the watertable that is rich in metallic sulphides poses little harm when undisturbed; however, exposure to the oxidizing atmosphere (e.g., through construction and mining) can result in a significant increase in acid drainage. The enhanced runoff results from the increased surface area available for oxidation. This runoff can contaminate water supplies, resulting in degradation of aquatic environments within the system. Figure 1.4 shows a stream receiving runway drainage in the area of the HIA. The rusty discoloration in the water results from hydrated oxides or sulphates of iron and aluminum, a by-product of acid drainage, as predicted in Eq. 1.5. Similar iron hydroxides residue occur near Petpeswick Lake off Highway 107, 40 km east of Halifax (Fig.1.5). The highway construction occurred on similar sulphide-rich black slate of the Halifax Formation.

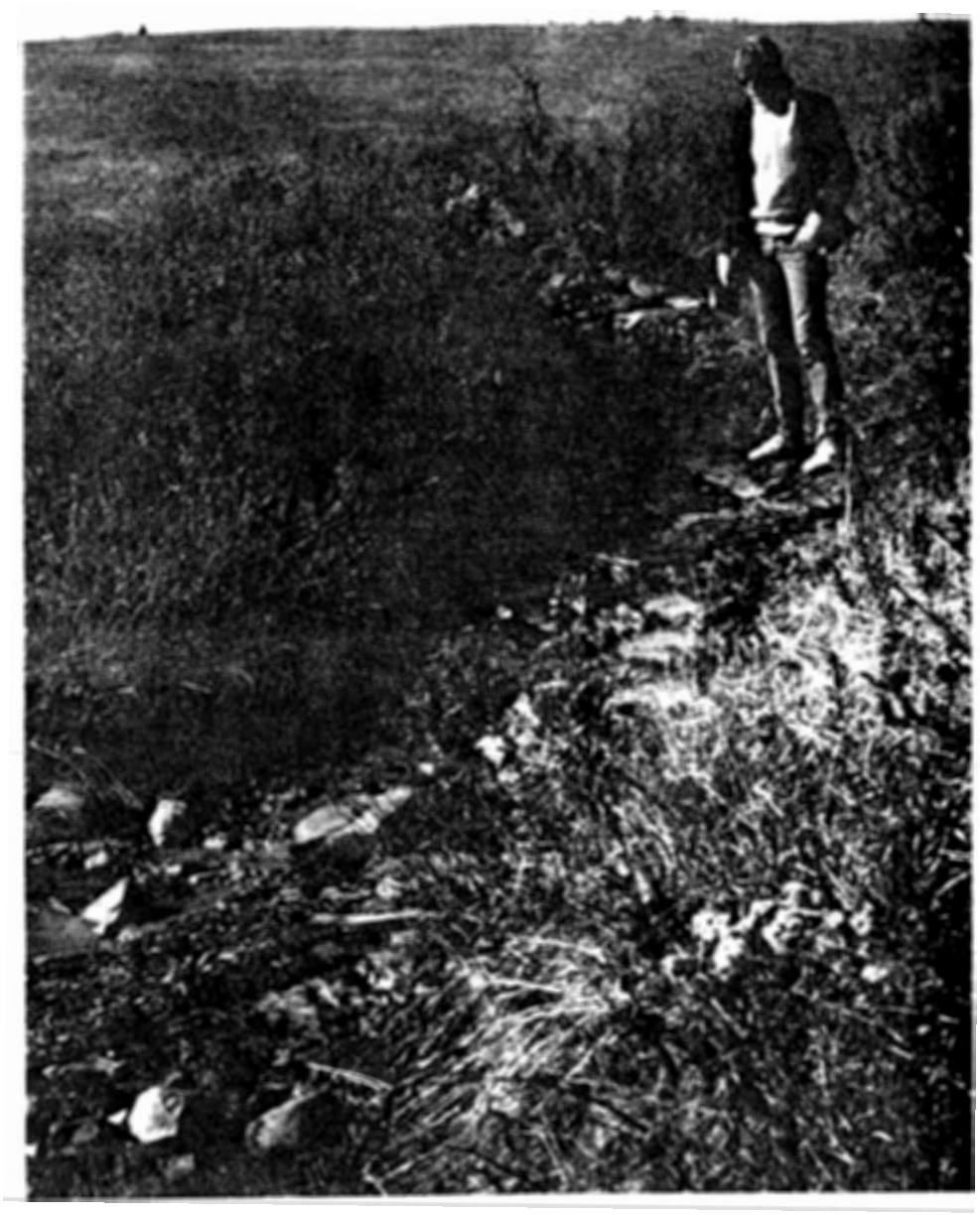

Figure 1.4 Steam draining from the Halifax International Airport runway containing residue of hydrated oxides or sulphates of iron and aluminum.

Figure 1.5 Residues of hydrated oxides or sulphates of iron and aluminum near Petpeswick Lake off Highway 107, 40 km east of Halifax.

1.4 Previous Work

The potential production of sulphuric acid determines the risk of acid drainage. This risk depends on the sulphide content and neutralizing capacity of the rock. Past assessments of this risk of drainage from the Halifax Formation slates have assumed the predominant sulphide mineral present in the rock to be pyrite. However, ongoing mineralogical studies (MacInnis et al. in preparation) showed the predominant sulphide-bearing mineral to be pyrrhotite, not pyrite, in representative slates from the Halifax International Airport. Pyrite and marcasite are less abundant. Therefore, disturbing pyrrhotite-rich rocks may initially cause higher rates of acid drainage production than originally expected since pyrrhotite oxidation rates are significantly faster than pyrite. That is to say, rocks with the same amount of S locked in pyrite may decay more gradually and pose less environmental risk.

Aeromagnetic mapping of the area surrounding the HIA shows high magnetic anomalies along the Halifax Formation (Fig.1.6). Previous studies in other areas of the Halifax Formation suggest that pyrrhotite is the predominant magnetic mineral (King 1994; Haysom 1994; Schwartz and Broome 1991). This thesis tests the possibility that the areas of high magnetic anomaly indicate high potential risk areas for acid drainage.

1.5 Approach and Methodology

Magnetic susceptibility readings were taken from a series of powdered core samples drilled from the Halifax International Airport. Polished thin sections, from representative samples of wide magnetic susceptibility range, were then studied using

Figure 1.6 High resolution aeromagnetic residual total field map of the Halifax International Airport and surrounding area. The areas in purple indicate zones of high magnetic signature (Nova Scotia Dept. of Mines, 1982).

?

GSC

petrographic and ore microscopic techniques. The microprobe was used to perform micro analyses on the mineral phases identified, and the distribution of specific elements were mapped within the samples. The sulphide mineralogy of the samples was compared to the magnetic susceptibility readings to determine a possible correlation.

1.6 Organization

This thesis begins with a statement explaining the purpose and scope of the report and presents a general understanding of acid drainage as well as a summary of previous work done on this topic. Chapter 2 deals with the history and current situation of acid drainage at the HIA. Chapter 3 explains the concept of magnetic susceptibility and presents susceptibility measurements of the HIA core. Chapter 4 provides a description of polished thin sections corresponding to the magnetic susceptibility measurements taken from this core. Chapter 5 correlates the data collected in Chapters 3 and 4. The final chapter draws conclusions from these results.

CHAPTER 2: ACID DRAINAGE AT THE HALIFAX INTERNATIONAL AIRPORT (HIA)

2.1 Location and Geologic Setting

The Halifax International Airport (HIA) is located on 972 ha. of land in the Atlantic uplands, 37 km north of Halifax. The airport was built on the highest point in the region, 145 m above sea level, situated on the topographic divide between the Bay of Fundy and the Atlantic Ocean where drainage originates on airport property as headwater streams affecting six different watersheds (Fig. 2.1). The HIA is located on a NE-SW trending, 2.5 km wide band of Halifax Formation slate, belonging to the Meguma Group (Fig. 2.2). The slate is highly fractured with visible sulphide mineralization concentrated along cleavage planes.

2.2 Acid Drainage at the Halifax International Airport

Acid drainage originating from the airport was responsible for the occurrence of massive fish kills in the various surrounding streams and degraded water supplies after major construction at the HIA disrupted black slates (Environmental Protection Service 1976; Thompson 1978) (Table 2.1). Severe fish kills occurred in the autumns following several summers of heavy construction. Increased acid (Fromm 1980) and high aluminum concentrations (Godfry 1989), known causes of fish kills, were likely causes for the massive fish kills that occurred at the airport.

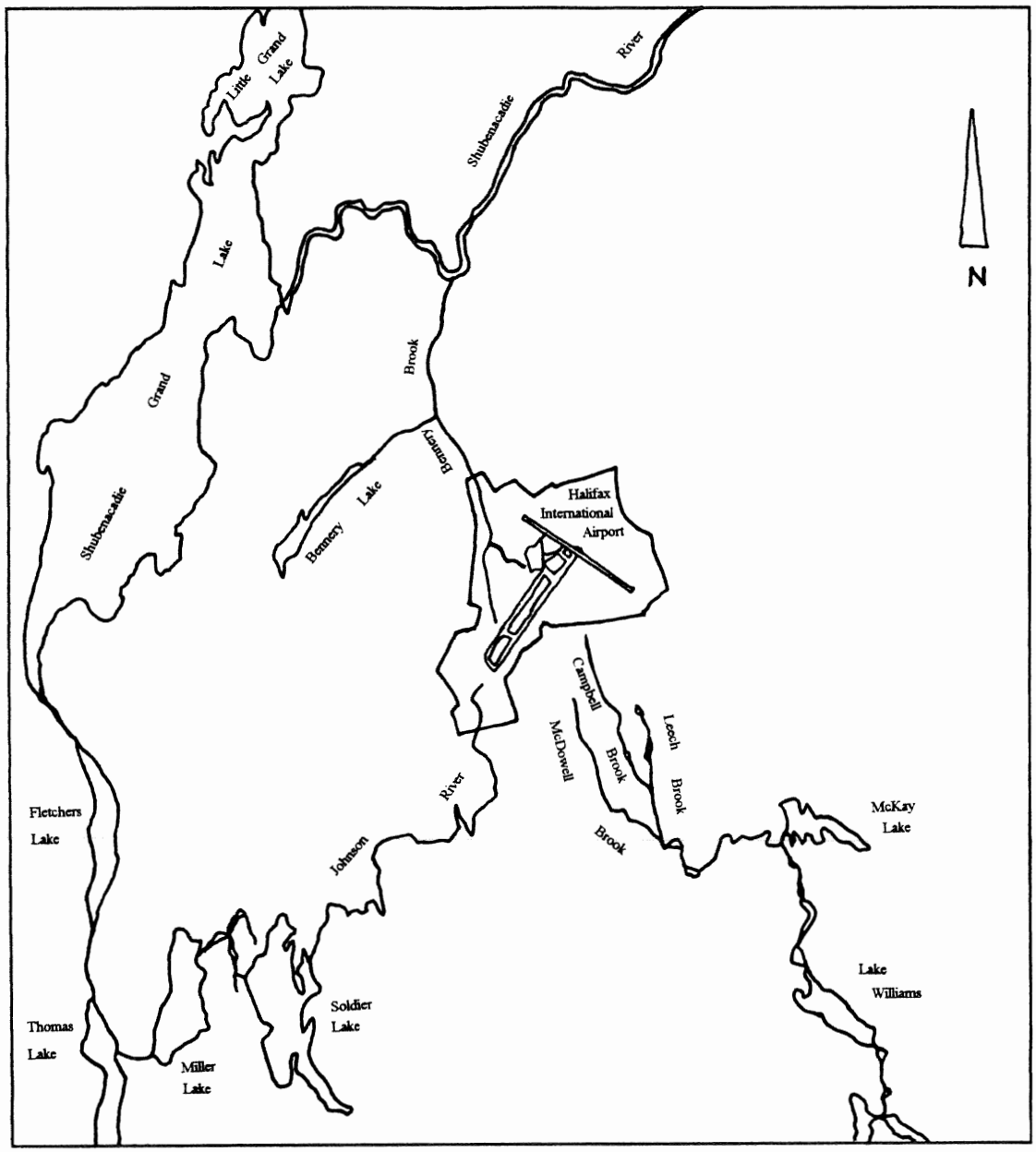

Figure 2.1 Major waterways draining the Halifax International Airport (Roberts 1986).

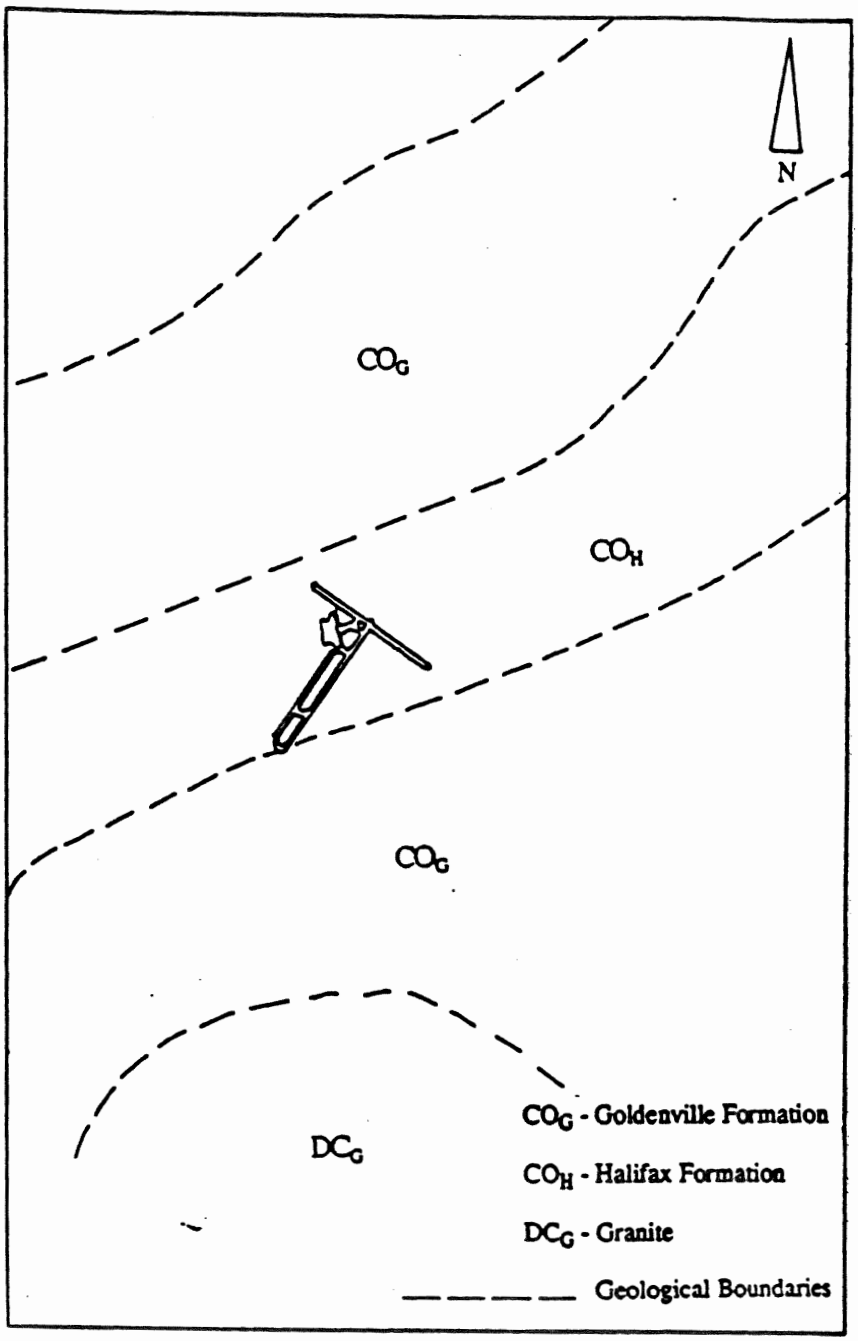

Figure 2.2 Geology of the Halifax International Airport and surrounding area (Roberts 1986).

Major Construction	Date	Major Fish Kills
Terminal and Runways	1957-1960	September, 1960
Imperial Oil	1959-1960	
IMP Hangar (large)	1959	
IMP Hangar (small)	1961	
Air Canada Hangar	1961	
Air Halifax Hangar	1961	October, 1961
Highways slate needs	1965	October, 1965
Avis Service Station	1966	September, 1966
Highway slate needs	1968	November, 1968
Halifax Flying Club	1970	
Mobil Oil Hangar	1972	
Highway Overpass	1974	August, 1974
Aircon Tank Farm	1975	October, 1975
EPA Hangar	1976 *	September, 1976

Table 2.1 Fish Kill History and Major Airport Construction Correlation (EPS 1976).

* The table extends only to 1976 but fish kills correlated with major construction have occurred on a regular basis up to the present.

The rate of oxidation of mineralized slates increases in the presence of a bacterium known as Thiobacillus Ferrooxidans (Temple and Colmer 1951; Silver and Ricey 1985; Erickson et al. 1985). The bacterium chemically bonds to the mineral surface via pilla or chemical bonds, using adhesion to accelerate the mineral oxidation process by enhancing direct enzymatic attack (DiSpirito et al. 1982). This bacterium is present in effluents from the HIA. (Ref. ?)

Much of the recent acid drainage at the Halifax International Airport originated from a 7 ha. mound of excavated slate referred to as the "waste rock pile". This pile accumulated in 1982, when taxiway construction removed 220,000 m^3 of overburden and 227,000 m^3 of sulphidic slate bedrock (Worgan 1987). The bedrock cut area was approximately 140 m long, 300 m wide, and 4.5 m deep. The waste rock pile began to generate large quantities of acid runoff, at an average pH of 3, within two months of the taxiway completion (Monenco 1983).

2.3 Response to the Situation of Acid Drainage at the HIA

In response to the situation of acid drainage, Transport Canada constructed a temporary lime treatment facility, at a cost of $500,000, in an attempt to neutralize the acid runoff. This system was not designed to treat large volumes and is not optimal as a long-term treatment facility. Initial estimates were that the acid drainage would cease within two years of the slate disturbance and the treatment plant would then be closed. After two years of treatment, however, the acidic runoff increased, with lower pH values and higher concentrations of dissolved metals reported (Porter Dillon 1985). The plant

operates at an annual cost of approximately $250,000; however, continual upgrading and/or a new system must be designed for treatment of the acid drainage problem. Another $800,000 was spent capping the waste pile with 75 cm of clay and 15 cm of topsoil to reduce the amount of drainage that requires treatment (Worgan 1987) .

2.4 Summary

The Halifax International Airport was built on "high-risk" Halifax Formation slate. The massive fish kills in the area surrounding the airport occurred as a direct result of disruption of this sulphide-rich bedrock during construction. However, the acid drainage problem in Nova Scotia is certainly not restricted to the Halifax International Airport. The potential risk for acid drainage continues to present a serious problem for future construction throughout the province. Properly locating the high-risk areas is essential since remediation of the disrupted slates is limited and costly. The next chapter introduces magnetic susceptibility as a method for locating such areas in the future.

CHAPTER 3: MAGNETIC SUSCEPTIBILITY

3.1 Introduction

This chapter introduces the concept of magnetic susceptibility, contains susceptibility measurements for both powdered and solid HIA core samples, and discusses the methods for obtaining these data. Susceptibility measurements along the entire length of the drill core also provide evidence for the magnetic heterogeneity of the core.

3.2 Overview of Magnetic Susceptibility

Minerals achieve their magnetic characteristics at the atomic level, through the 3-dimensional positioning of the electrons. The combination of an orbital magnetic moment resulting from orbital angular momentum, and a spin magnetic moment resulting from the electron spin, produces a net magnetic moment such that for a given angular momentum the spin gives twice the magnetic moment of the orbit (Jiles 1991). The spin of the electron in space behaves as a small magnet and produces a magnetic field while moving around its orbit. Two electrons on the same orbital will have opposing spins which results in a zero net magnetic moment. However, a magnetic moment exists if the electron is unpaired, with the strength of the magnetic moment being proportional to the number of unpaired electrons on each orbital (Klein and Hurlbut 1993).

Magnetic susceptibility is the response of a magnetic material to a magnetic field and is a measure of the ability of that material to take on induced magnetism. Induced magnetization is a temporary phenomenon produced by an external magnetic field.

Magnetic susceptibility does not refer to remnant magnetization, in which a material remains permanently magnetic independent of any external magnetic field. Magnetic susceptibility, χ , is the ratio of the intensity of the induced field to that of the field which produces it, and is simply the magnetizability of a substance. It is defined by the expression

$$\boldsymbol{M} = \chi \mathbf{H} \qquad (4.1)$$

where $\boldsymbol{M}$ is the *induced magnetization* a material acquires when exposed to a *magnetic field,* **H** (Jiles 1991). Both $\boldsymbol{M}$ and **H** are usually in Systeme Internationale units of amperes/meter. These units cancel out, leaving χ dimensionless.

3.3 Magnetic Susceptibility of the Halifax Formation

Schwartz and Broome (1991) has shown that elongate positive magnetic anomalies, parallel to the strike of bedding, occur over the Halifax Formation, and that pyrrhotite is the dominant magnetic constituent and the probable cause of the anomalies. Schwartz and Broome (1991) determined an average susceptibility of 6×10^{-3} SI for the Halifax Formation.

3.4 Methods

Magnetic susceptibility measurements were taken of both solid and powdered HIA core in an attempt to determine the relationship between the amount of pyrrhotite in the core and its susceptibility reading. All susceptibility measurements contained in this report were taken using the MS-3 Magnetic Susceptibility Bridge and the Exploranium KT-5 hand-held susceptibility meter.

The MS-3 Magnetic Susceptibility Bridge (Fig. 3.1) was used to make susceptibility measurements of the powdered core samples. It operates on the principle that the introduction of a magnetic material into the sample holder will alter the mutual inductance between two coils of wire. This inductance differential determines the impedence of the material, ΔR, in ohms. Fourteen powdered core samples were placed into cylindrical glass containers which were in turn placed into the sample holder of the MS-3 Magnetic Susceptibility Bridge to measure the impedence of the sample. The impedence was then multiplied by a conversion factor of 4.9 to determine the volume susceptibility, k_{powder}. The conversion factor was determined by measuring the impedence and volume of $MnSO_4 \cdot H_2O$ of known susceptibility, and comparing it to the impedence and volume of unknown susceptibility. The volume susceptibility of the powder was multiplied by the density (σ) ratio to determine the mass susceptibility, χ, of the slate. The density of the powder was determined by weighing the sample and recording its dimensions in the container. The average density of the slate was assumed to be 2.4 g/cm^3 (Kearey and Brooks 1991). The following equations summarize the steps for converting ΔR to χ_{slate}.

$$\Delta R \times 4.9 = k_{powder} \tag{3.2}$$

$$k_{powder} \times \sigma_{slate} / \sigma_{powder} = \chi_{slate} \tag{3.3}$$

The precision with which the zero position can be set on the dial determines accuracy of the instrument. An error of 0.5-5 ohms is expected.

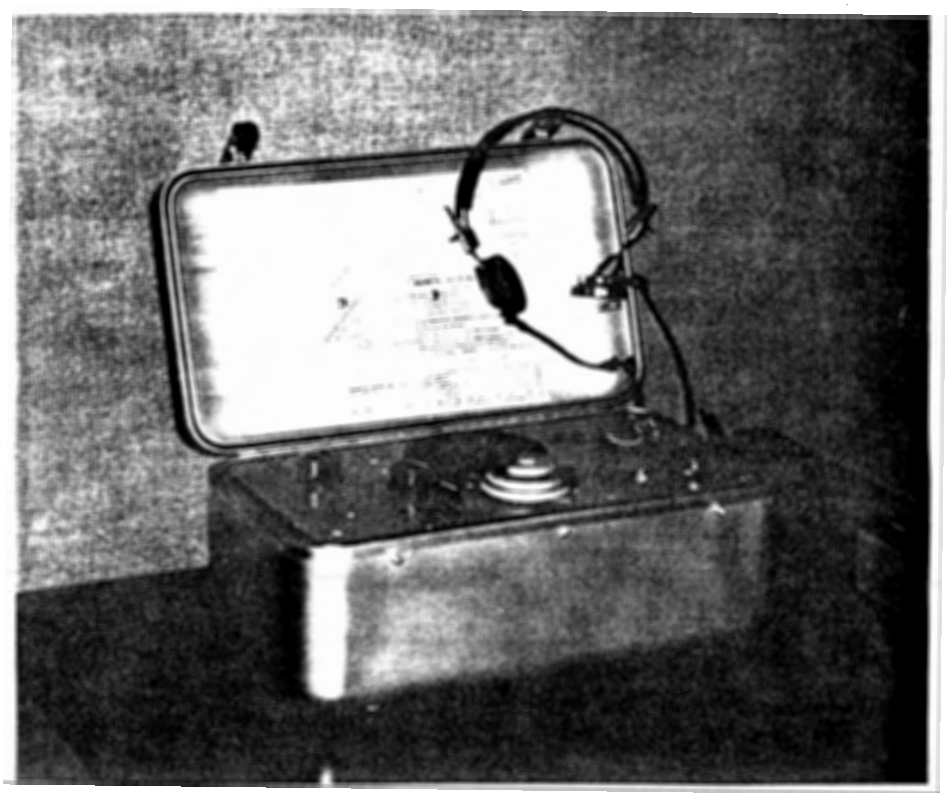

Figure 3.1 MS-3 Magnetic Susceptibility Bridge

The Exploranium KT-5 susceptibility meter (Fig. 3.2) was used to take susceptibility measurements of the solid HIA core samples. This hand-held instrument consists of a flat measuring coil which measures the frequency of an LC oscillator of 10 kHz, situated within the active face of the instrument. The frequency difference determines the magnetic susceptibility which is displayed digitally. The "true" susceptibility depends on the size and geometrical shape of the rock being measured. Magnetic susceptibility readings decrease as the distance between the sample and the KT-5 increases, and as the size of the sample decreases. The KT-5 manual recommends that for accurate susceptibility readings, the core diameter should not be less than 60 mm. The airport core samples measured, however, have a diameter of 36 mm. Measurements taken on the cylindrical surface of the core rather than a flat surface
decrease the intensity of the reading. However, the cylindrical surface provided a larger surface area for measurements with the KT-5 than the much smaller end diameters. The smaller size and cylindrical shape of the core will generate smaller susceptibility values than "true" values but, for this experiment, only relative values within the core are important; therefore, readings from the Magnetic Susceptibility Bridge and the KT-5 are not comparable.

This study used seven drill holes taken from the airport property. Much of the drill core has been damaged and broken into fragments 5 - 200 cm long and has freqently split apart along cleavage planes. The KT-5 was set on a continuous reading mode to take continuous measurements along the core at approximate intervals of 8 cm. The average

Figure 3.2 Exploranium KT-5 magnetic susceptibility meter.

length of each broken core fragment was 130 mm. The diameter of the KT-5 face is 100 mm. All core samples chosen for measurement either met or exceeded this diameter. The susceptibility measurements were plotted against the distance (Appendix A) to determine the distribution of pyrrhotite. The peaks and troughs on the graphs demonstrate the heterogeneity of the slate and show that, if pyrrhotite is the cause of these anomalies, then its distribution throughout the core is highly variable. Magnetic susceptibility values of some core fragments varied greatly from one side of the core to the other. This discrepancy is attributed to the limited depth of penetration of the susceptibility meter. Thin sections come from the same part of the core as the magnetic susceptibility measurements to ensure that the magnetic susceptibility reading is representative of the mineralogy.

3.5 Data from Solid and Powdered Core Samples

The average susceptibility of the Halifax Formation core from the HIA used in this study is 2.5×10^{-3} SI for the solid core samples and 3.2×10^{-4} SI for the powdered core samples. The lower values may be due to regional variability; however, these values are most likely the result of oxidation. The sulphide content of these samples may have decreased over the last nine years, as a result of oxidation, resulting in overall lower susceptibility values. The geometry of the core being measured may also generate lower susceptibility values. However, only the relative values within the suite are required to determine a correlation. Thirteen corresponding polished thin sections were cut from the core samples before they were powdered.

Table 3.1 shows magnetic susceptibility measurements from thirteen powdered

Sample	Description	Magnetic Susceptibility ($\times 10^{-5}$ SI)
HIAC-60	black slate	133.33
HIAC-52	black slate	79.29
HIAC-57	bleached siltstone	76.53
HIAC-56	silty slate	76.53
HIAC-50	grey siltstone	58.81
HIAC-23	grey siltstone	19.35
HIAC-59	black slate	0
HIAC-53	grey siltstone	0
HIAC-4	black slate	0
HIAC-54	black slate	0
HIAC-72	grey-black slate	0
HIAC-22	grey silty slate	0
HIAC-58	black slate	0
HIAC-51	black slate	0

Table 3.1 Magnetic susceptibility measurements of powdered HIA core samples.

core samples.

Five samples of solid core (Appendix B) were used to determine the mineralogy and corresponding magnetic susceptibility values. These particular samples were chosen to represent a wide range of low to abundant visible sulphide mineralization. Correspondingly, the magnetic susceptibility values cover a broad range from a low of near zero to a high of around 4×10^{-3} SI. Susceptibility measurements were taken from several different areas on each core fragment. The surface of the core in the photographs is the area where the measurements were taken. Twelve polished thin sections were cut from these exact locations. Table 3.2 outlines the magnetic susceptibility readings of these solid core samples. Samples showing visible amounts of pyrrhotite along the cleavage planes gave considerably higher susceptibility values than samples of black slate showing little or no pyrrhotite mineralization. Chapter 4 and Appendix C contain analyses of the thin sections corresponding to the susceptibility readings of both the powdered and solid core samples.

3.6 Conclusion

Magnetic susceptibility readings of the solid core show a general relationship between the amount of visible sulphide minerals observed in the core and the magnitude of the susceptibility reading generated. Chapter 5 uses the data contained in this chapter to test for correlation with measured pyrrhotite abundances.

Sample	Description	Magnetic Susceptibility (x 10^{-3} SI)
BH-20-1.1	grey siltstone - pyrrhotite lenses visible along cleavage planes	2.50
BH-20-1.2	grey siltstone - pyrrhotite lenses visible along cleavage planes	2.30
BH-20-1.3	grey-black slate	1.55
BH-20-1.4	grey siltstone - pyrrhotite lenses visible along cleavage planes	4.07
BH-20-2.1	grey siltstone - abundant pyrrhotite lenses visible along cleavage planes	3.75
BH-20-2.2	grey siltstone - pyrrhotite lenses visible along cleavage planes	1.95
BH-20-4.1	grey siltstone - abundant pyrrhotite lenses visible along cleavage planes	4.48
BH-20-4.2	grey siltstone - pyrrhotite lenses visible along cleavage planes	3.40
BH-16-1	black slate	0.07
BH-8-1	grey siltstone - pyrrhotite lenses visible along cleavage planes	2.20
BH-8-2	grey siltstone - pyrrhotite lenses visible along cleavage planes	2.30
BH-8-3	grey siltstone - pyrrhotite lenses visible along cleavage planes	1.41

Table 3.2 Sample descriptions and magnetic susceptibility measurements of Halifax International Airport core using the Exploranium KT-5. Pyrrhotite tends to be concentrated in the grey siltstone of the Halifax Formation rather than the black slate.

CHAPTER 4: SULPHIDE MINERALOGY

4.1 Introduction

The purpose of this chapter is to describe the sulphide mineralogy of the HIA samples through microprobe analyses and reflected light microscopy, and to determine the amount of pyrrhotite in each thin section. The calculated percentages are then compared with the corresponding magnetic susceptibility measurements determined in the previous chapter.

4.2 Methods

In selecting samples for this study, an effort was made to choose samples that are representative of common styles of sulphide mineralization in the HIA slate. Polished thin sections of core samples were chosen to represent a broad range of magnetic susceptibility readings with low, moderate, and abundant amounts of visible pyrrhotite. The sulphide mineralogy of these samples was studied under reflected light using a petrographic microscope. The percentage of pyrrhotite in each thin section was then determined through computer imaging and point counting (Tables 4.1 and 4.2). This method does not take into account the very fine-grained pyrrhotite. In addition, all of the opaques in the thin section were assumed to be pyrrhotite. Analyses in reflected light showed that the abundance of other opaques is insignificant. A microprobe analysis was also performed for identification and composition of the mineral phases. Selected

Sample	% Pyrrhotite
BH-20-4.1	4.6
BH-20-4.2	4.3
BH-20-1.2	3.4
BH-8-3	3.2
BH-20-1.4	3.1
BH-8-2	3.0
BH-20-1.1	2.0
BH-8-1	1.4
BH-20-2.2	0.7
BH-20-1.3	0.2
BH-16-1	0

Table 4.1 Area abundance of pyrrhotite in selected thin section samples from the solid core taken from the Halifax International Airport.

Sample	% Pyrrhotite
HIAC-52	10.2
HIAC-50	5.3
HIAC-57	3.5
HIAC-59	3.1
HIAC-23	2.6
HIAC-56	2.2
HIAC-58	1.2
HIAC-53	1.2
HIAC-72	0.5
HIAC-60	0
HIAC-04	0
HIAC-51	0
HIAC-54	0

Table 4.2 Area abundance of pyrrhotite in selected thin section samples corresponding with powdered core samples taken from theHalifax InternationalAirport.

microprobe data with descriptions of the corresponding photomicrographic figures are located in Appendix C.

4.3 Sulphide Mineralogy and Geochemistry

Sulphides comprise 0-10% modal abundance in the samples studied from the Halifax International Airport. Pyrrhotite is by far the predominant sulphide mineral. The slates contain less than 1% pyrite. Arsenopyrite and chalcopyrite are present but are far less abundant. The sulphide mineralogy study is, therefore, limited to pyrrhotite and pyrite as they are the primary minerals involved in acid drainage generation.

Pyrite (FeS_2) has a cubic structure and belongs to the isometric system. Pyrite displays relatively little substitution of other metals for Fe, other than small amounts of Ni, Co, and Mn. In hand sample, pyrite appears metallic brassy yellow. Pyrite is completely opaque and is pale brassy yellow in reflected light (Fig. 2A). In some HIA core samples, pyrite replaces pyrrhotite with typical "birds-eye" texture. The large euhedral grains in some samples most likely formed during metamorphic recrystallization (Fig. 18A). Thin veinlets of ribboned pyrite indicate mechanical strain during metamorphism (Fig. 23A).

Pyrrhotite ($Fe_{1-x}S$, x = 0-0.17) consists of a slightly distorted hexagonal close-packed array of S with Fe atoms in sixfold coordination between the layers of S. The ratio Fe:S is slightly less than one but may vary depending on the number of Fe atom sites that are vacant (Nesse 1991). Pyrrhotite commonly assumes the hexagonal form ($\sim Fe_9S_{10}$) at temperatures above 300°C, but normally reverts to the monoclinic variety ($\sim Fe_7S_8$) at lower temperatures. All of the pyrrhotite in the HIA samples is monoclinic, with no

nonmagnetic Fe_9S_{10} intergrowths. In hand sample, pyrrhotite appears as metallic bronze-yellow, but may have a brownish or reddish cast. Like pyrite, pyrrhotite is opaque but may be distinguished from pyrite in reflected light by its darker, bronze colour (Fig. 22A). In HIA core samples, pyrrhotite most commonly occurs as granular aggregates commonly in the form of elongate lenses (Fig. 10A). X-ray diffraction techniques showed that 73% of all pyrrhotites are mixtures of "$Fe_{1-x}S$ hexagonal" and "$Fe_{1-x}S$ monoclinic", 5% are troilite + $Fe_{1-x}S$ hexagonal, 13% are pure hexagonal and only 9% are pure "$Fe_{1-x}S$ monoclinic" (Arnold 1966). The average stoichiometry for pyrrhotite from the airport core samples is $Fe_{7.058}S_{8.000}$ (MacInnis et al., in preparation).

4.4 History of Sulphide Formation at the Halifax International Airport

The protolith of the black slates of the Halifax Formation is black shale which in turn formed from deep-sea black muds. Pyrite probably formed in these black muds as a result of bacterial reduction of seawater sulphate present in the pore spaces of deep-sea sediment during early diagenesis. However, much of this pyrite has been altered to pyrrhotite as a result of prograde metamorphism. The prograde metamorphic reaction, by desulphidation, is as follows (Ferry 1981):

$$\underset{\text{pyrite}}{2\,FeS_2} + \underset{\text{fluid}}{2\,H_2O} + \underset{\text{graphite}}{C} \;\text{-->}\; \underset{\text{pyrrhotite}}{2\,FeS} + \underset{\text{fluids}}{2\,H_2S + CO_2} \qquad (4.1)$$

The reverse reaction of pyrrhotite to pyrite has also taken place during retrograde metamorphism by local remobilization of pyrrhotite to form pyrite porphyroblasts. Figure

8A shows a pyrrhotite grain in which the edges have reverted to pyrite. Retrograde metamorphism forms pyrite, which is more oxidized than pyrrhotite, according to the following redox reaction (Hall and Fallick 1988):

$$\underset{\text{pyrrhotite}}{8\,FeS} + 5\,CO_2 + \underset{\text{fluids}}{2\,H_2O} \rightarrow \underset{\text{pyrite}}{4\,FeS_2} + \underset{\text{fluids}}{CH_4} + \underset{\text{siderite}}{4\,FeCO_3} \qquad (4.2)$$

Prograde metamorphism led to a reduction whereas retrograde metamorphism led to an oxidation (Hall and Fallick 1988).

4.5 Summary

Monoclinic pyrrhotite dominates the sulphide mineralogy of the samples used in this study. The pyrrhotite formed in the slate as a result of prograde metamorphism and is primarily concentrated along the cleavage planes. Appendix C contains microphotographs along with brief descriptions of these thin sections.

CHAPTER 5: CORRELATION OF MAGNETIC SUSCEPTIBILITY WITH MINERALOGY

5.1 Introduction

The previous two chapters discussed the mineralogy and corresponding magnetic susceptibility of the selected samples. This chapter combines both sets of data to determine a possible correlation between these two variables.

5.2 General Observations

Samples of core containing abundant visible pyrrhotite generated much higher magnetic susceptibility readings than samples having little or no visible pyrrhotite. Figure 5.1 shows a typical core fragment of the Halifax Formation from the HIA. The grey siltstone in the upper portion of the core contains abundant visible pyrrhotite mineralization and generates susceptibility values of 3.25 - 4.10 x 10^{-3} SI. The black slate in the lower portion of the core contains no visible pyrrhotite and generates much lower susceptibility readings of 0.06 - 0.11 x 10^{-3} SI.

5.3 Correlation Results from Solid HIA Core Samples

Table 5.1 lists the modal percentages of pyrrhotite and the magnetic susceptibility values for each sample of solid HIA core. Figure 5.1 plots and fits the values with a regression line according to the "least-squares fit" method. The regression line shows that magnetic susceptibility increases with increasing abundance of pyrrhotite according to

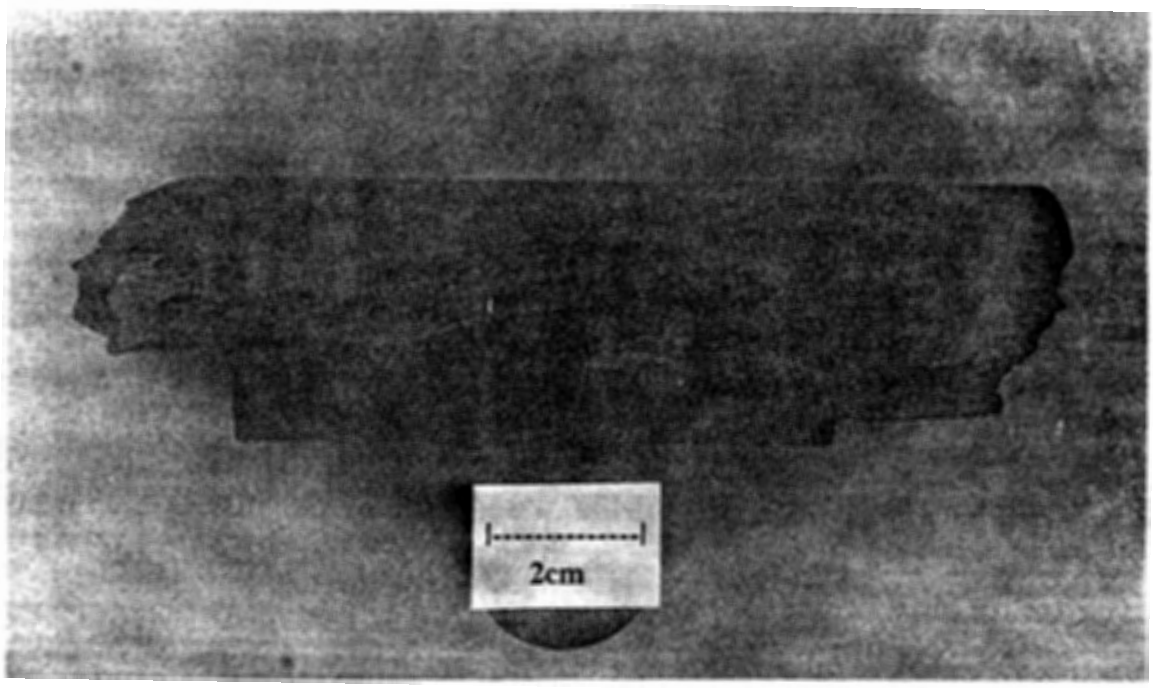

Figure 5.1 Halifax Formation core fragment, BH-8-5, from the HIA showing grey siltstone with abundant sulphide mineralization (top) and black slate with no visible pyrrhotite (bottom).

Sample	Magnetic susceptibility ($x 10^{-3}$ SI)	% Pyrrhotite
BH-20-4.1	4.48	4.6
BH-20-4.2	3.40	4.3
BH-20-1.2	2.30	3.4
BH-8.3	1.41	3.2
BH-20.1.4	4.07	3.1
BH-8-2	2.30	3.0
BH-20-1.1	2.50	2.0
BH-8-1	2.20	1.4
BH-20-2.2	1.95	0.7
BH-20-1.3	1.55	0.2
BH-16-1	0.07	0

Table 5.1 Area percentage of pyrrhotite in the thin section from the solid core samples with corresponding magnetic susceptibility values.

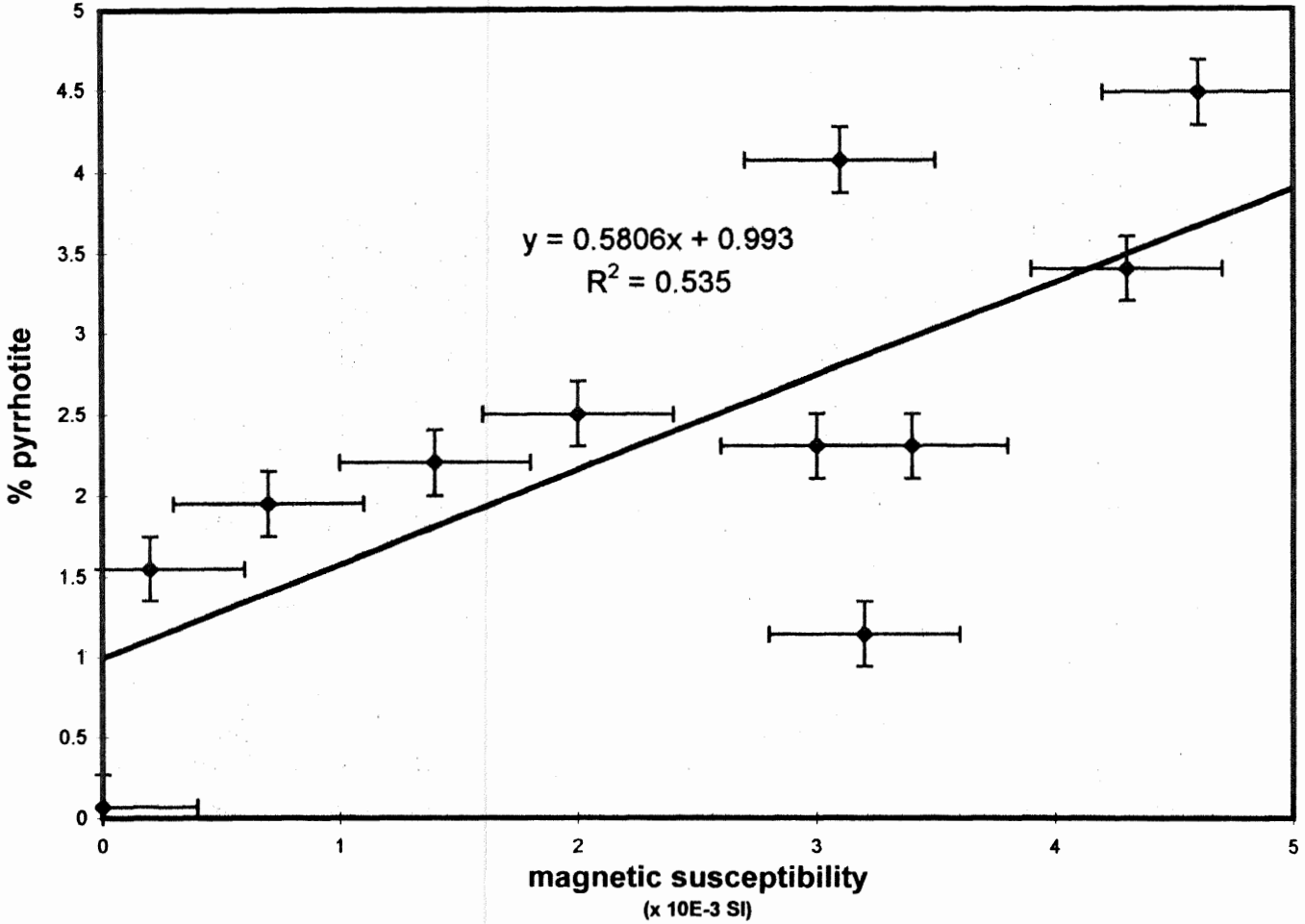

Figure 5.2 The relationship between the area abundance of pyrrhotite in thin section and magnetic susceptibility of solid HIA core samples.

the equation:

$$y = 0.5806x + 0.993 \quad (5.1)$$

where y is the percent of pyrrhotite and x is magnetic susceptibility. A relatively low correlation coefficient (R^2) of 0.535 for the regression line occurs because some points deviate significantly from the general trend. These deviations may have resulted from sampling errors in data collection. The depth of penetration of the KT-5 Magnetic Susceptibility Meter is low. As a result, thin sections which needed to be cut at least three millimetres below the cylindrical surface of the core might not have been an exact representation of the magnetic susceptibility. The nonuniform distribution of the pyrrhotite also lowers the likelihood of the thin section matching the magnetic susceptibility reading. The trendline was constructed to compensate for the measuring errors and heterogeneity of the core.

By substituting for y and x in Equation (5.1), a formula for determining acid drainage potential may be given by,

$$\% \text{ Po} = 0.5806\,\chi + 0.993 \quad (5.2)$$

where the percentage of pyrrhotite is directly proportional to the amount of acid runoff that may be potentially generated through oxidation, and χ is magnetic susceptibility ($\times 10^{-3}$ SI). Future studies should test the validity of this equation by reproducing it with a larger data set.

The core should also be at least 60 mm in diameter so that the KT-5 can take measurements on the flat surfaces of the ends rather than the cylindrical surface. In this way, thin sections could then be cut closer to the surface where the susceptibility measurement are taken. Also, several susceptibility measurements should be taken at each location to generate error bars.

5.4 Correlation Results from Powdered HIA Core Samples

Table 5.3 lists the relationship between magnetic susceptibility and pyrrhotite abundance for the powdered core samples. The plot of these values (Fig. 5.3) shows that there is no conclusive relationship between these two variables. The lack of correlation probably arose from the powdering of the core samples which converts a heterogeneous sample to a homogeneous sample. The polished thin sections represent the percentage of pyrrhotite in very localized areas; however, reducing the heterogeneous core to powder mixes these areas with the rest of the core which may alter the overall percentage of pyrrhotite. For example, if a thin section were cut along a layer rich in pyrrhotite, it would have a relatively high percentage of pyrrhotite. However, if this layer of pyrrhotite was an isolated occurrence in a relatively pyrrhotite-poor core sample, then homogenizing the sample would result in an overall lower abundance of pyrrhotite and, consequently, a lower magnetic susceptibility reading. Therefore, the high percentage of pyrrhotite, as indicated by the thin section, would not correspond with the low magnetic susceptibility value.

Oxidation of the powder may also help to explain the lack of correlation. The

Sample	Magnetic Susceptibility ($x 10^{-5}$ SI)	% Pyrrhotite
HIAC-52	79.29	10.2
HIAC-50	58.81	5.3
HIAC-57	76.53	3.5
HIAC-59	0	3.1
HIAC-23	19.35	2.6
HIAC-56	76.53	2.2
HIAC-58	0	1.3
HIAC-53	0	1.2
HIAC-72	0	0.5
HIAC-60	133.33	0
HIAC-04	0	0
HIAC-51	0	0
HIAC-54	0	0

Table 5.3 Percentage of pyrrhotite in the powdered core samples

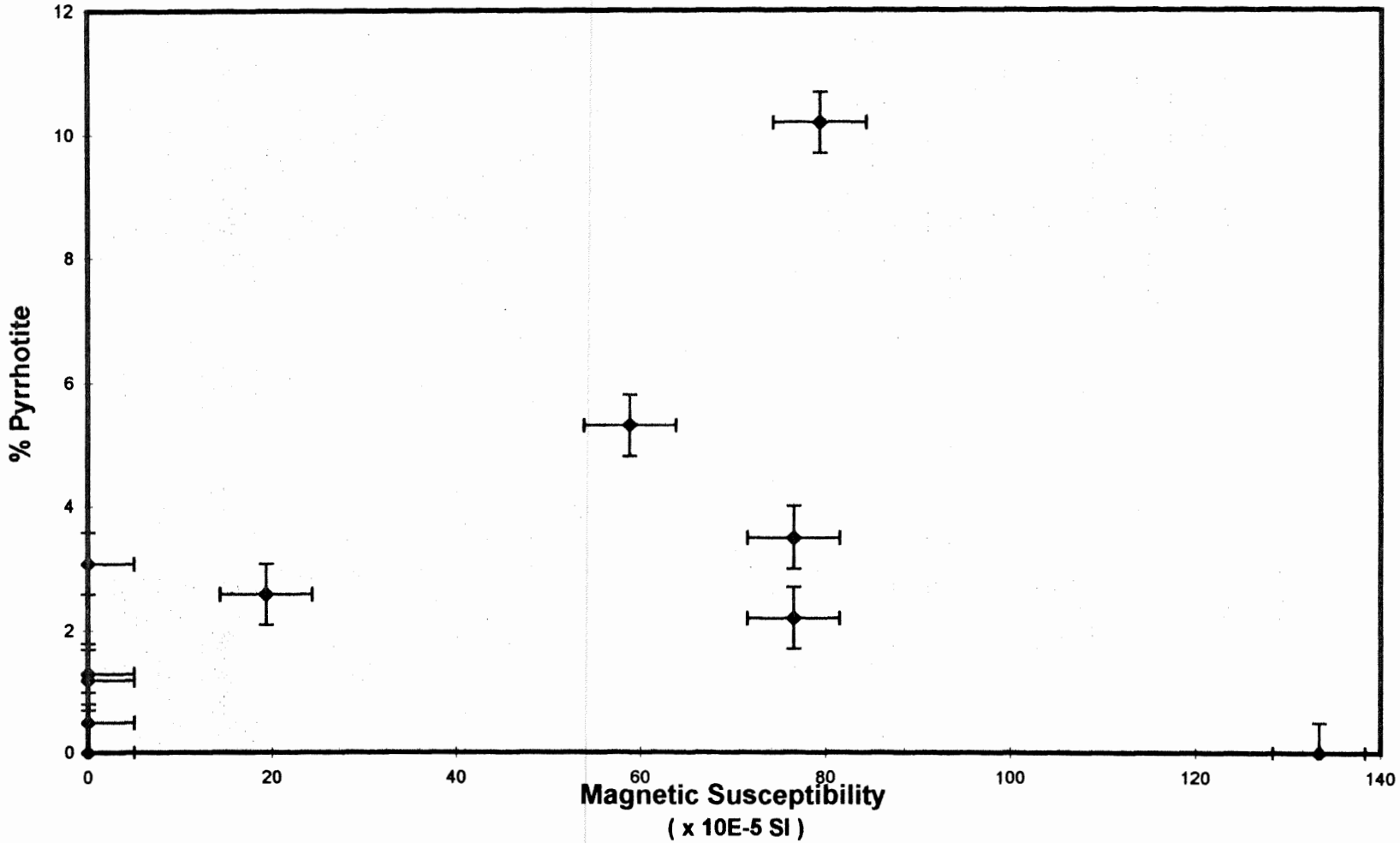

Figure 5.3 The relationship between the are abundance of pyrrhotite in thin section and magnetic susceptibility of powdered core samples.

core that was powdered in 1986 was compared to fresh powder to determine evidence of oxidation. The pyrrhotite was removed from the powder with a magnet and was examined under a binocular microscope. The pyrrhotite in the older powder appeared quite tarnished when compared to the pyrrhotite in the fresh powder, indicating that the powders had indeed experienced oxidation.

One possible method for correcting this lack of correlation would be to magnetically separate the pyrrhotite and other magnetic minerals from fresh powder so that the wt% of pyrrrhotite could be plotted against the bulk susceptibility. X-ray diffraction of heavy mineral concentrates should also be done.

5.5 Summary

Although the relationship between pyrrhotite abundance and magnetic susceptibility of the powdered samples was inconclusive, the solid core samples showed a positive correlation. From this correlation, Equation (5.2) was generated which may determine the potential risk for acid drainage. For this equation to be more conclusive, larger sets of data need to be generated to substantiate this data set. Chapter 6 provides a more detailed conclusion and gives recommendations for further study.

CHAPTER 6 : CONCLUSIONS AND RECOMMENDATIONS

Magnetic susceptibility and mineralogy data for the Halifax Formation core samples from the Halifax International Airport were analyzed to determine if there was a correlation between the two sets of data. Results of the data from the powdered core samples were inconclusive. Although no correlation was found between susceptibility and pyrrhotite abundance, measuring errors may have significantly reduced the correlation coefficient. The powdered core was subjected to a period of oxidation; as a result, the sulphide content of these samples may have decreased. In addition, crushing the heterogeneous core into a homogeneous powder may have produced very different pyrrhotite concentrations from the values indicated by the thin section. One possible method for correcting this lack of correlation would be to separate the heavy minerals from the powder so that the weight percent of Fe could be plotted against the bulk susceptibility. X-ray diffraction of heavy mineral concentrates should also be done. Another method would be to remove magnetic pyrrhotite from the powder with a magnet, and weigh it.

The solid core samples, however, generated a weak positive correlation coefficient ($R^2 = 0.535$). Magnetic susceptibility increased in response to increasing pyrrhotite content. The deviations from the general trend probably resulted from sampling errors during data collection. The small size and cylindrical measuring surface of the core caused lower susceptibility readings. Thin sections needed to be cut at least three millimeters below the cylindrical surface; therefore, the measuring surface and the corresponding thin section would slightly differ. For this reason, the thin section may not have been an exact representation of the susceptibility because of

the limited depth of penetration of the KT-5 Susceptibility Meter. The heterogeneity of the core may have also reduced the accuracy with which the thin sections could represent the pyrrhotite content. Future studies should test this correlation by attempting to reproduce it with a larger data set. The core should be at least 60 mm in diameter so that the KT-5 can take measurements on the flat surfaces of the ends of the core rather than the cylindrical surface. In this way, thin sections could be cut closer to the surface where susceptibility measurements are taken. Several susceptibility measurements should be taken at each location to generate error bars. Clearly, more data are required to determine a definitive correlation for the prediction of acid drainage.

References

Arnold R. G. 1966. Mixtures of hexagonal and monoclinic pyrrhotites and the measurements of the metal content of pyrrhotite by X-ray diffraction. American Mineralogist., **51**: 1221-1227.

Baker, M. 1975. Inactive and abandoned underground mines - water pollution prevention and control. U.S. Environmental Protection Agency, EPA 440/9-75-007.

Barnes, H.L. and, Romberger. 1968. Chemical aspects of acid mine drainage. Juvenile Water Pollutant Control Federation, **40**: 371-84.

Environmental Protection Service, Atlantic Region. 1976. A report on the causes of fish kills in the Shubenacadie River at Enfield, Nova Scotia. Environmental Services Branch.

Erickson, P.M., Kleinmann, R.L., and Onysk, S.J. 1985. Control of acid mine drainage by application of bacterial materials. Control of Acid Mine Drainage, Proceedings of a Technical Transfer Seminar, Bureau of Mines: Information Circular 9027.

Ferry, J.M. 1981. Petrology of graphitic sulphide-rich schists from south-central Maine: an example of desulphidation during prograde regional metamorphism. American Mineralogist, **66**: 908-930.

Fromm, P.O. 1980. A review of some physiological and toxicological responses of freshwater fish to acid stress. Environmental and Biological Fisheries, **5**: 79-83.

Gotfry, A. 1989. Aluminum and acid: a sinister synergy. Canadian Research, June/July: 10-11.

Graves, M.C. and Zentilli, M. 1988. The lithochemistry of metal-enriched coticules in the Goldenville-Halifax transition zone of the Meguma Group, Nova Scotia; in Current research, Part B, Geological survey of Canada, Paper, Paper 88-1B, 251-261.

Jiles, D. 1991. Introduction to magnetism and magnetic minerals. Chapman and Hall, New York, NY.

Hall, A.J. and Fallick, A.E. 1988. A sulphur isotope study of iron sulphides in the Late Precambrian Dalradian Easdale Slate Formation, Argyll, Scotland. Mineralogical Magazine, **52**: 483-490.

Haysom, S.J. 1994. The opaque mineralogy, petrology, and geochemistry of the Meguma Group metasediments, Rawdon Area, N.S. (Thesis). Saint Mary's University. Halifax, N.S.

Horne, R.J. 1992. Preliminary report on the geology of the Rawdon area. Mines and Energy Branches Report, **93-1**: 61-67.

Kearey, P. and Brooks, M. 1991, An introduction to geophysical exploration, second edition. Blackwell Scientific Publications.

King, M.S. 1994. Magnetic mineralogy and susceptibility of the north-central Meguma Group: implications for the interpretations for the aeromagnetic total field, first derivative, and second derivative. N.S. Department of Natural Resources. Mines and Energy Branches, Open File Report 94-004.

Klein, C. and, Hurlbut, C.S.Jr. 1993. Manual of mineralogy. John Wiley & Sons, Inc.

Lund, O.P., 1987. Acid drainage from mineralized slate at the Halifax International Airport. In Proceedings: Acid Mine Drainage Workshop/Seminar, Environment Canada, Halifax, Nova Scotia, 137-165.

MacInnis, I., Pasava, J., Graves, M.C. Zentilli, M., (In preparation). Mineralogy and geochemistry of iron sulphides in Meguma slates: source of acid drainage at the Halifax International Airport, Nova Scotia, Canada.

Monenco Ltd. 1983. Halifax airport hydrology study, phase II. Prepared for Transport Canada.

Nesse, W.D. 1991. Introduction to optical mineralogy. Oxford University Press, New York, Oxford.

Nicholson, R.V. 1994. Iron-sulfide oxidation mechanisms: laboratory studies. Environmental Geochemistry of Sulfide Mine-Wastes, MAC Short Course, Waterloo, Ontario: 163-183.

Nordstrom, D.K. 1982. Aqueous pyrite oxidation and the consequent formation of secondary iron minerals. Acid Sulfate Weathering; SSSA Special Publication #10: 37-56.

Nova Scotia Department of Mines. 1979. Geology map of Nova Scotia. Compiled by Duncan Keppie.

Nova Scotia Research Foundation. 1985. The evaluation of some geophysical methods for the detection of shallow sulphide mineralization. Prepared ~~by~~ for Environment Canada. Dartmouth, Nova Scotia.

Porter Dillon Ltd. 1985. Environmental study of the Salmon River watershed in the vicinity of the Halifax International Airport, Halifax, Nova Scotia. Consult Study for Transport Canada, March, 1985.

Schenk, P.E. 1970. Regional variation of the flych-like Meguma Group (lower Paleozoic) of Nova Scotia, compared to recent sedimentation off the Scotian Shelf. In: Flysch sedimentology in North America. Edited by J. Jajoie. Geological Association of Canada. Special Paper 7: 127-153.

Schenk, P.E. 1983. The Meguma Terrane of Nova Scotia - an aid to trans-Atlantic correlation. In Regional trends in the geology of the Appalachian-Caledonian-Hercynian-Mauritanide orogeny (ed. P.E. Schenk), NATO ASI Series C., **116**: 121-130.

Schwartz, E.J. and Broome, J. ~~1991~~ 1994. Magnetic anomalies due to pyrrhotite in Paleozoic metasediments in Nova Scotia, Eastern Canada, ~~Geological survey of Canada, Ottawa, Ont., Canada~~. Journal of Applied Geophysics, **32**: 1-10.

Silver, M. and Ritcey, G.M. 1985. Effects of iron-oxidizing bacteria and vegetation on acid generation in laboratory lysimeter tests on pyrite-containing uranium tailings. Hydrometallurgy, **15**: 255-264.

Temple, K.L. and Colmer, A.R. 1951. The autotrophic oxidation of iron by a new bacterium: Thiobacillus Ferrooxidans. Journal of Bacteriology. 62: 605-611.

Thompson, B.D. 1978. An investigation of Meguma bedrock leaching in the Shubenacadie-Stewiacke river basin. Shubenacadie-Stewiacke River Basin Board, Technical Report 8.

Waldron, J.W.F. and Graves, M. 1987. Preliminary report on sedimentology of sandstones, slates and bioclastic carbonate material in the Meguma Group, Mahone Bay, N.S. in Current Research, Part A, Geological Survey of Canada, Paper 87-1A: 409-414.

Worgan, J. 1987. Acid mine drainage in reactive slates "The Halifax International Airport Case" - The Transport Canada perspective. Proceedings of Acid Mine Drainage Seminar/Workshop, DSS Cat No. En 40-11-7/1987E: 50-58.

Appendix A

Magnetic Susceptibility Graphs of HIA Core

The KT-5 Magnetic Susceptibility Meter was used to take continuous measurements along the core at approximate intervals of 8 cm. Appendix A plots these meaasurements against the distance to determine the distribution of pyrrhotite. The peaks and troughs on the graphs demonstrate the heterogeneity of the slate and show that if pyrrhotite is the cause of these anomalies, then its distribution throughout the core is highly variable.

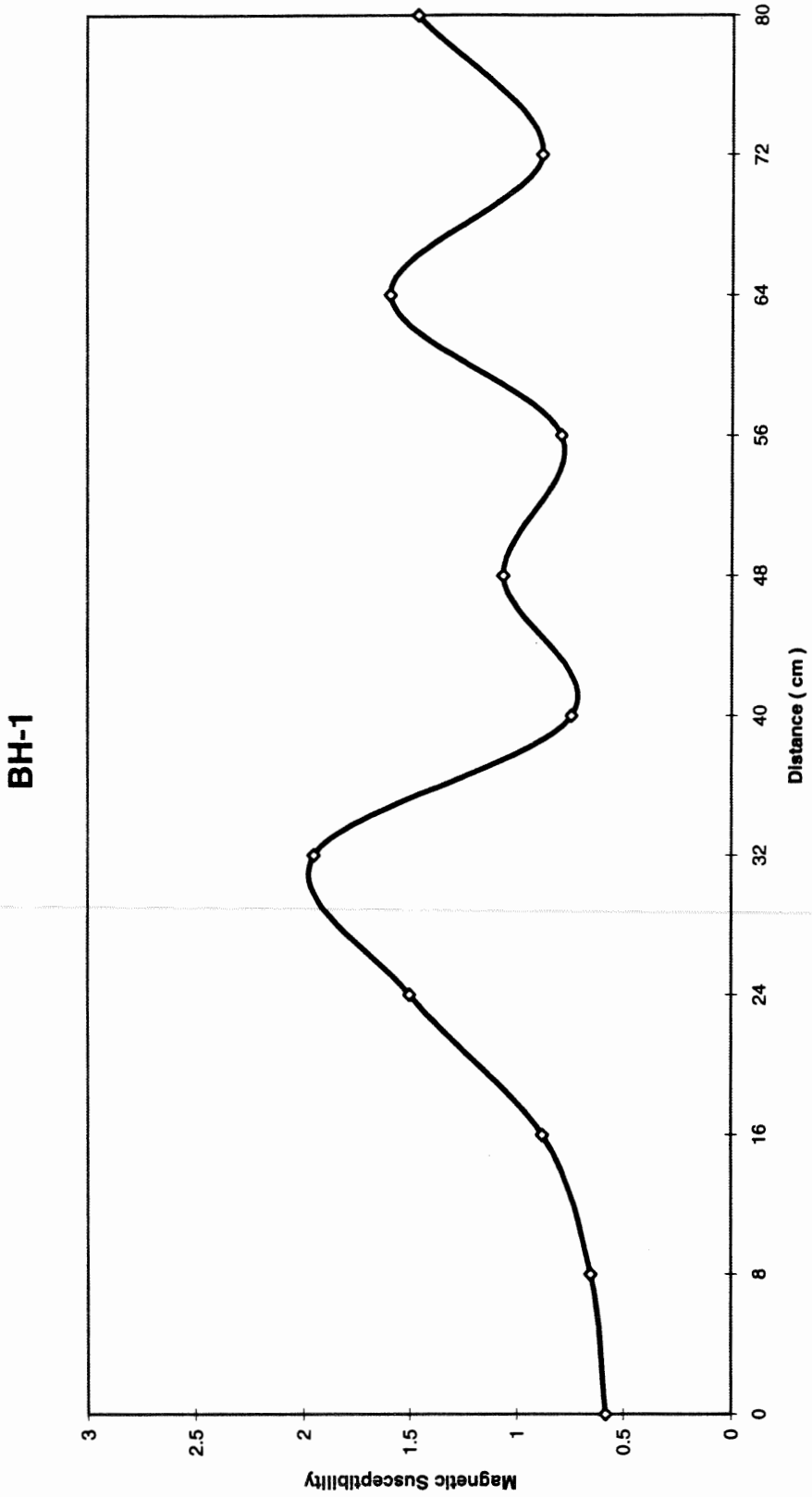
BH-1
Magnetic Susceptibility
3
2.5
2
1.5
1
0.5
0
0
8
16
24
32
40
48
56
64
72
80
Distance (cm)

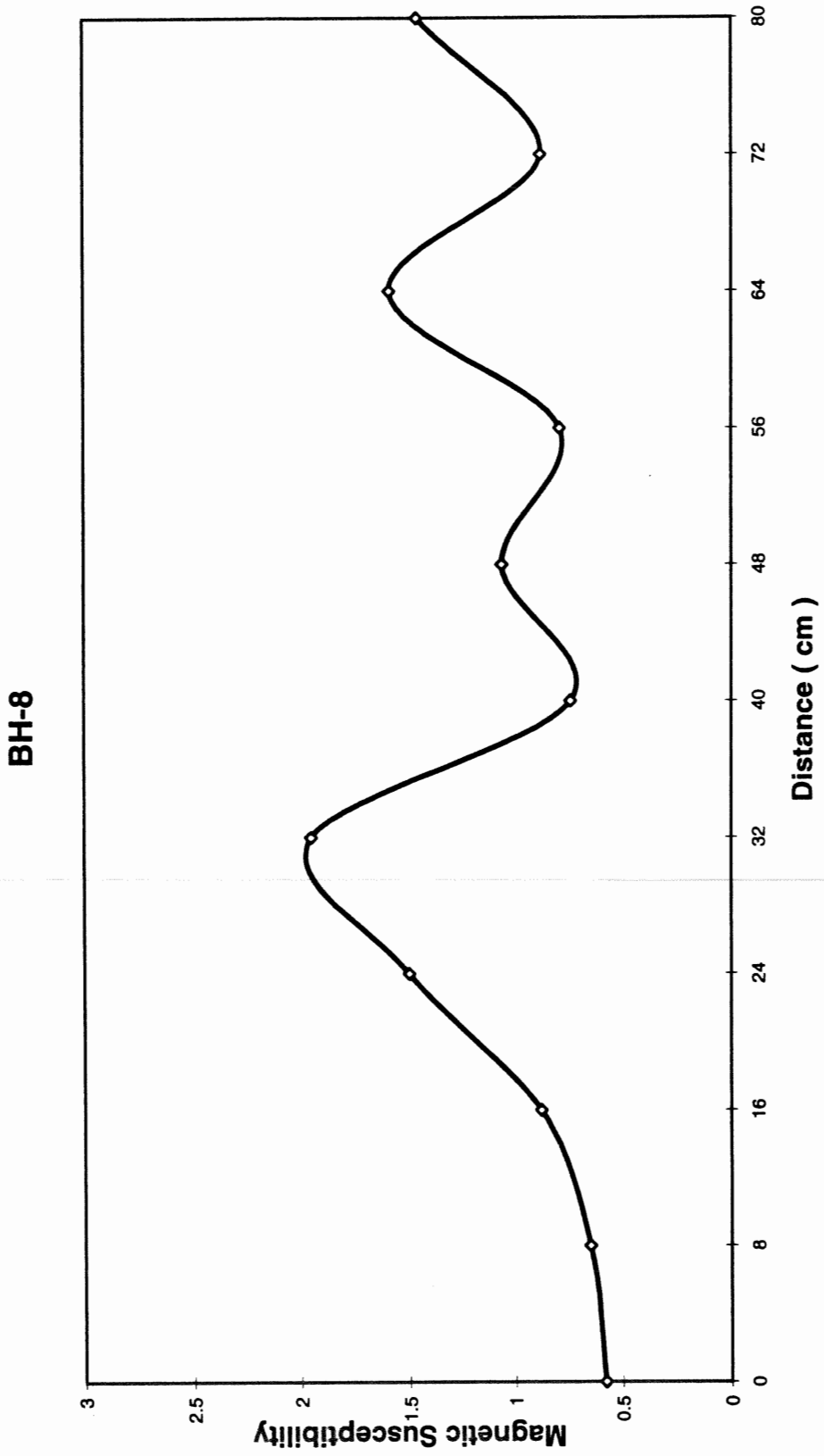
BH-8
Magnetic Susceptibility
Distance (cm)
0
0.5
1
1.5
2
2.5
3
0
8
16
24
32
40
48
56
64
72
80

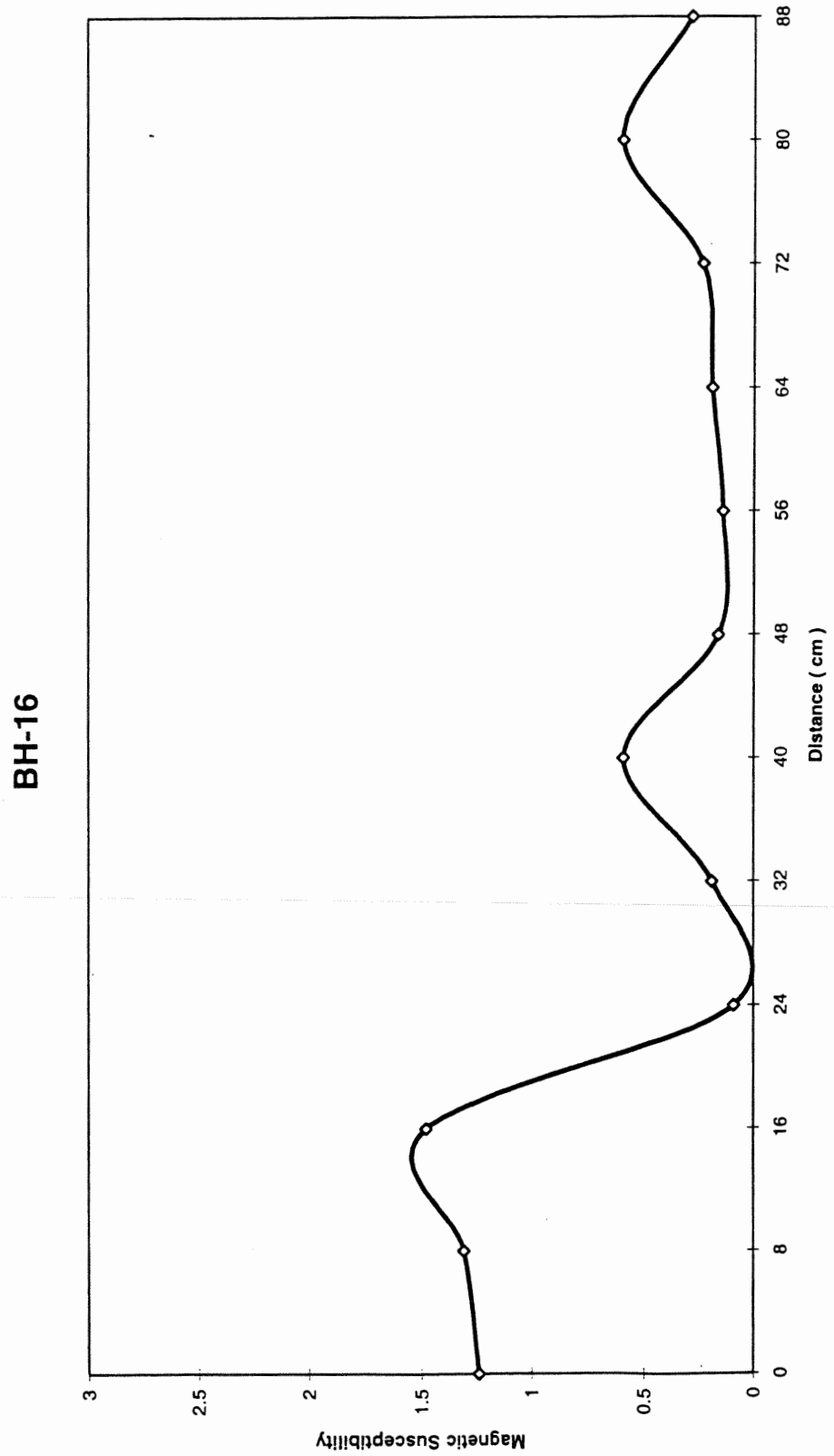
BH-16
Magnetic Susceptibility
0
0.5
1
1.5
2
2.5
3
Distance (cm)
0
8
16
24
32
40
48
56
64
72
80
88

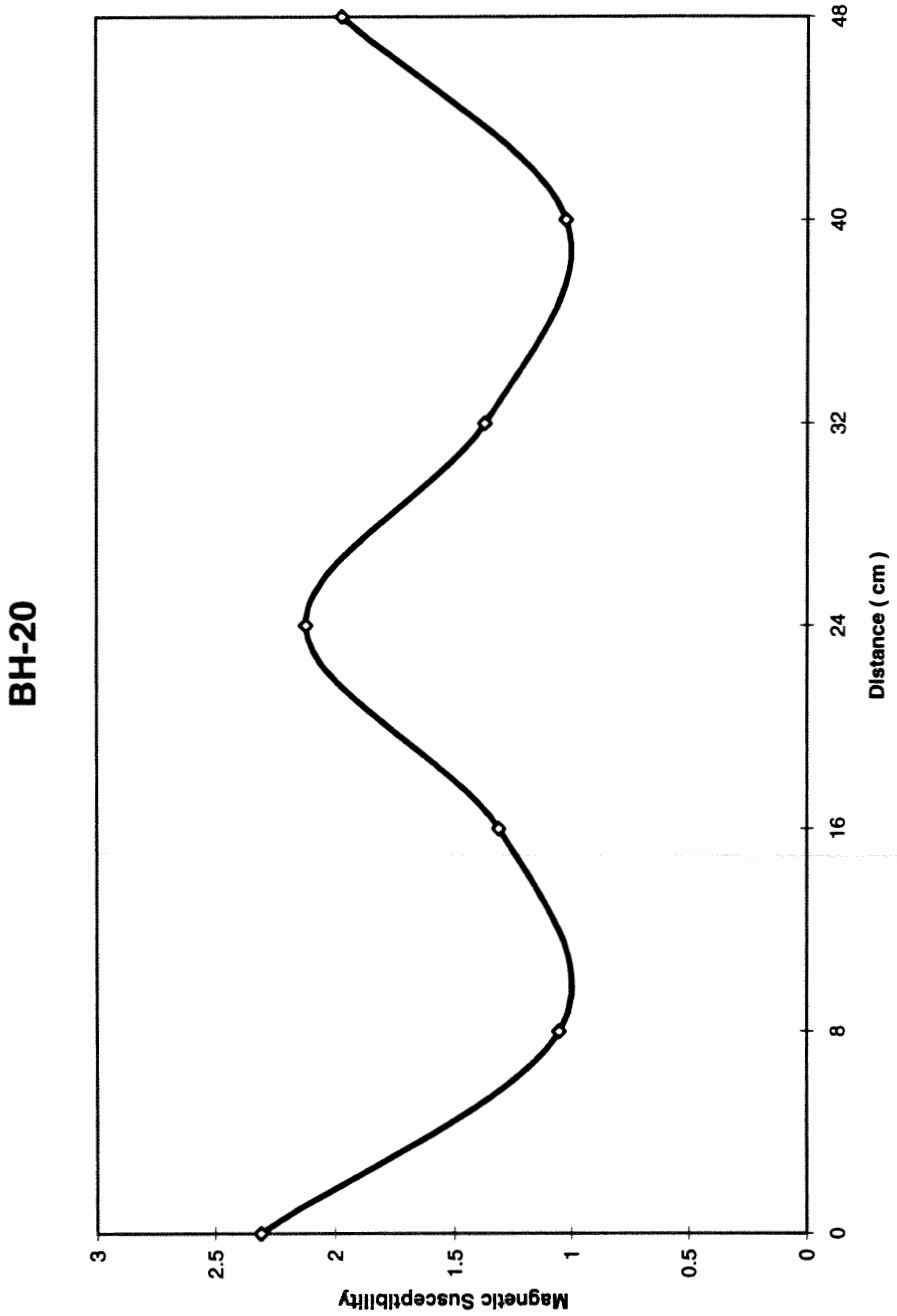
BH-20
Magnetic Susceptibility
3
2.5
2
1.5
1
0.5
0
0
8
16
24
32
40
48
Distance (cm)

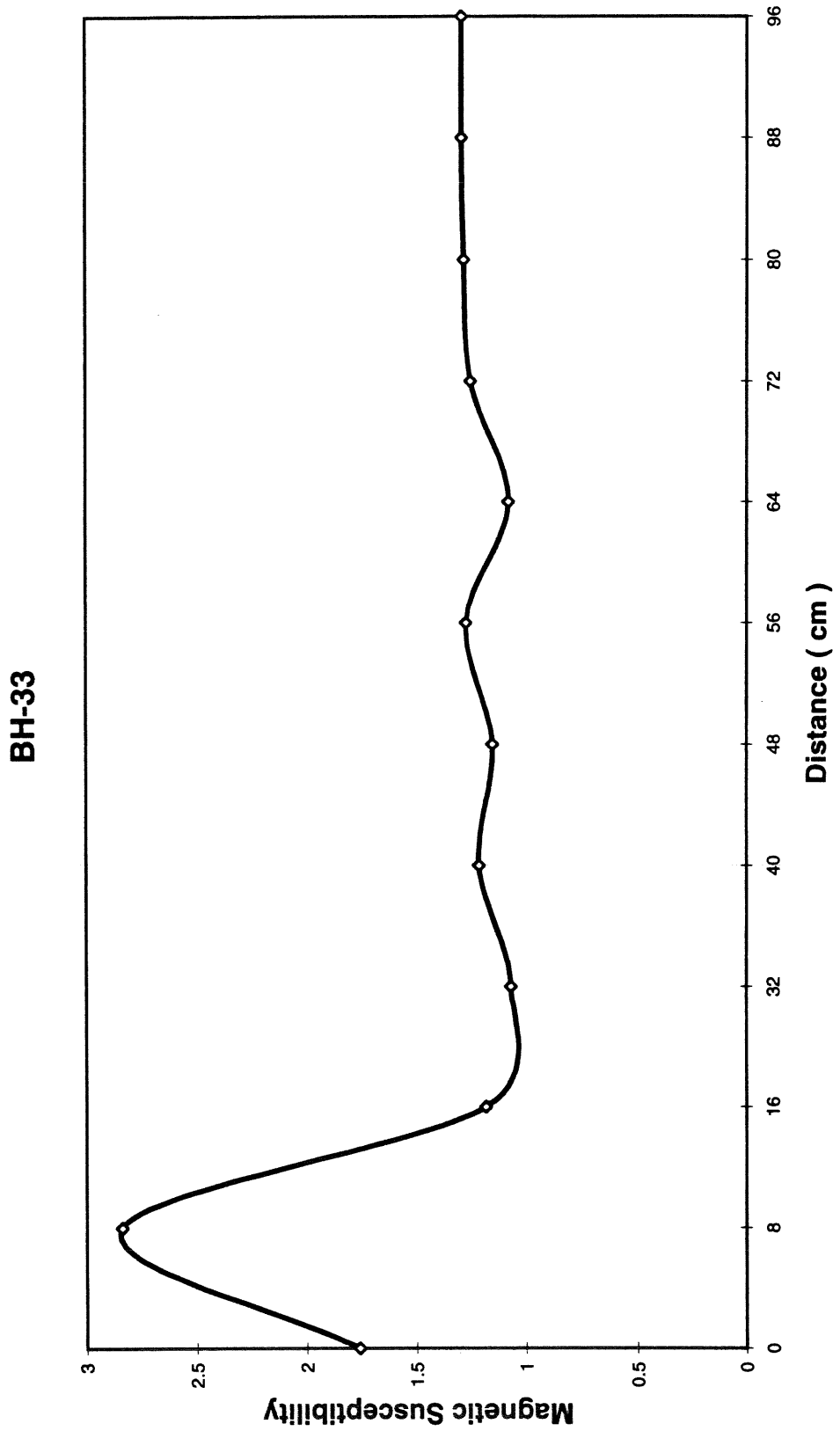
BH-33
Magnetic Susceptibility
3
2.5
2
1.5
1
0.5
0
0
8
16
32
40
48
56
64
72
80
88
96
Distance (cm)

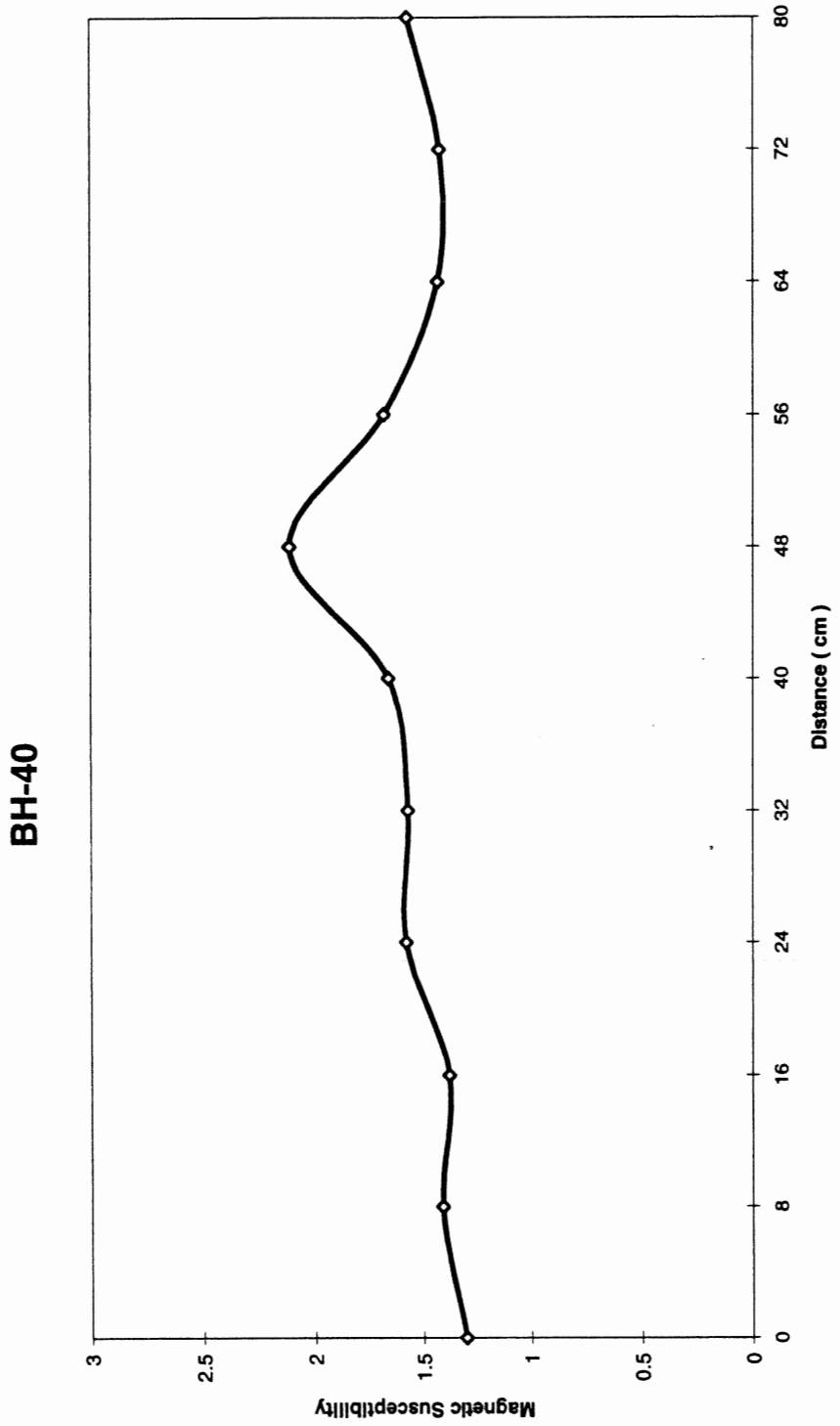
BH-40
Magnetic Susceptibility
0
0.5
1
1.5
2
2.5
3
Distance (cm)
0
8
16
24
32
40
48
56
64
72
80

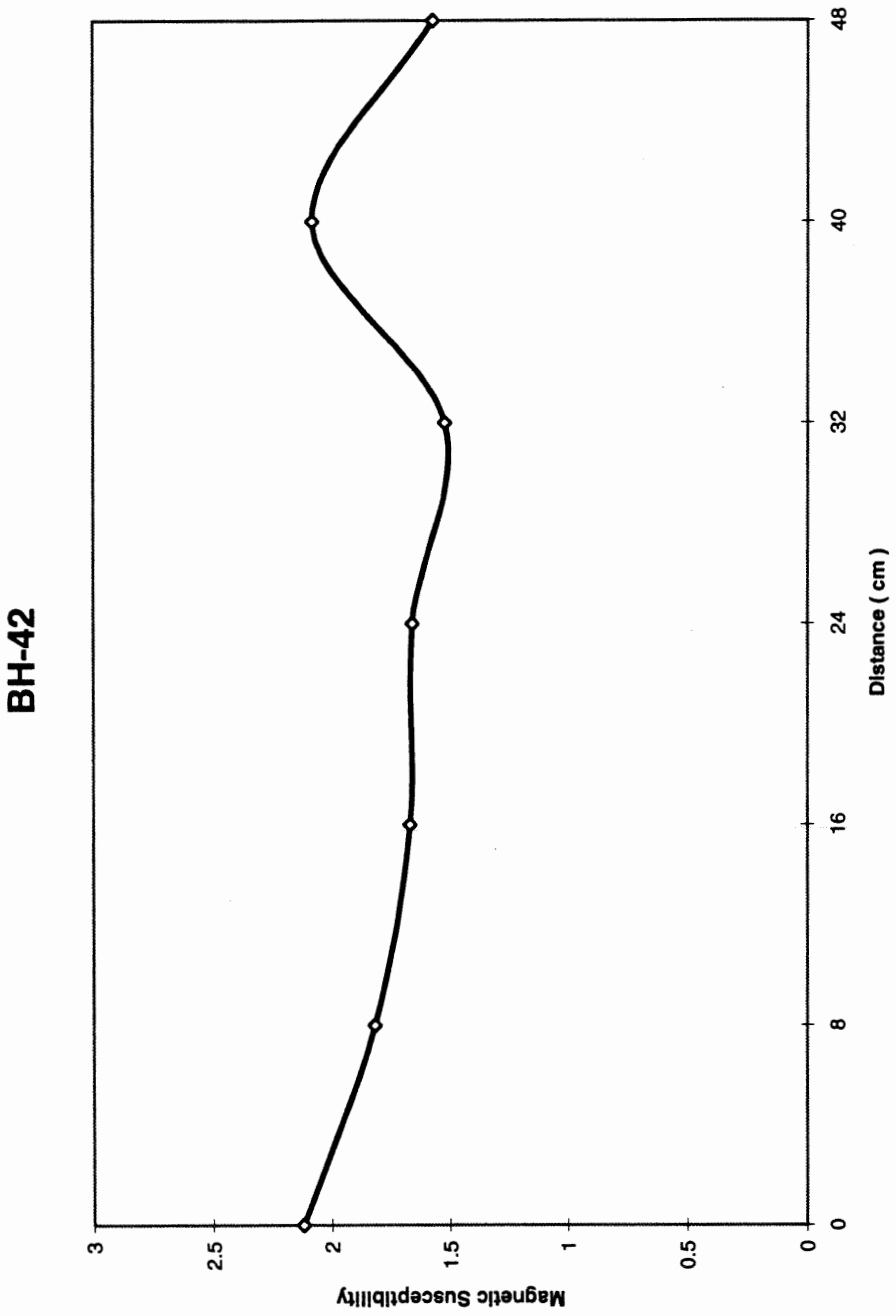
BH-42
Magnetic Susceptibility
3
2.5
2
1.5
1
0.5
0
0
8
16
24
32
40
48
Distance (cm)

Appendix B

Figures of Selected HIA Core Samples

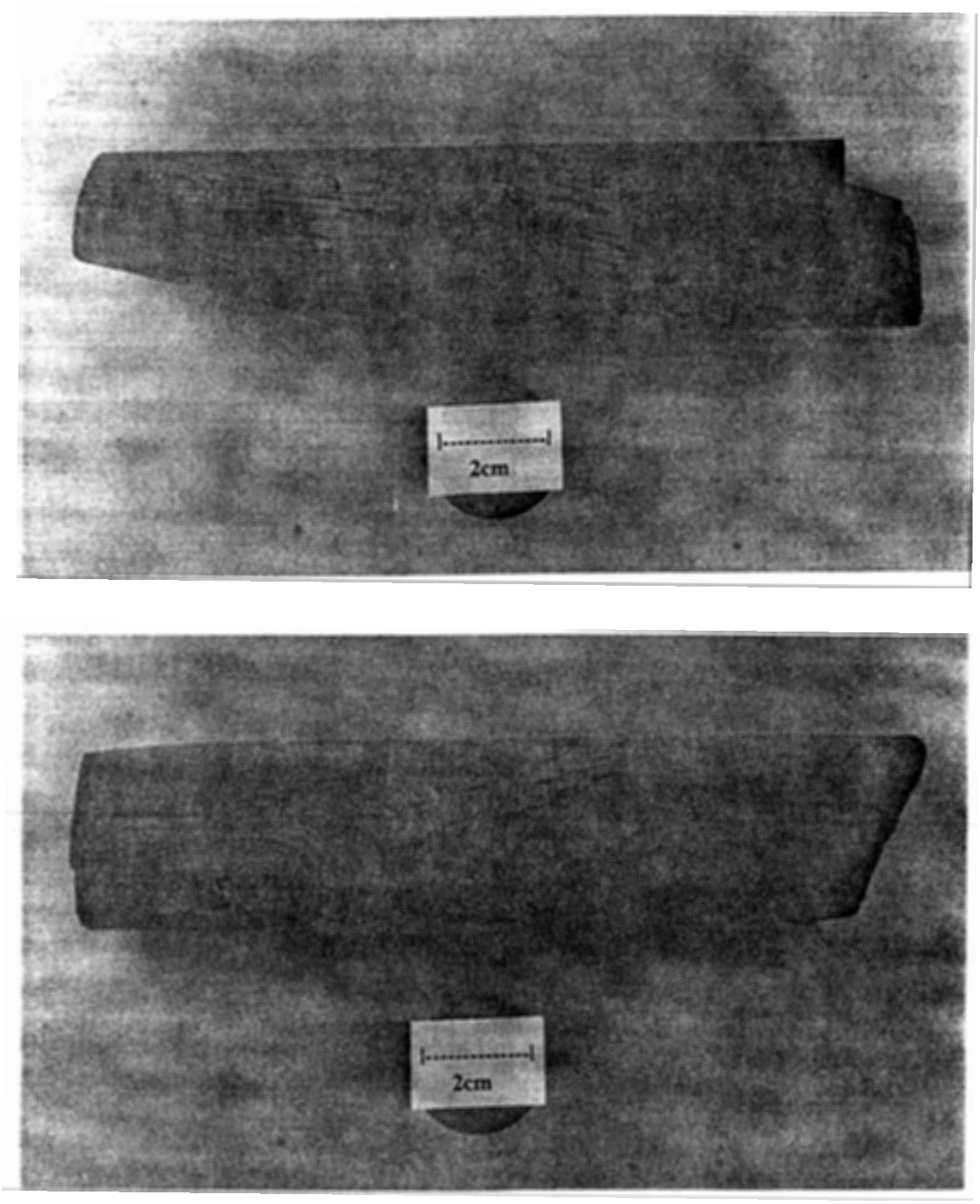

Figure 1B Sample BH-20-1.1 and BH-20-1.2 (top) and BH-20-1.3 and BH-20-1.4 (bottom).

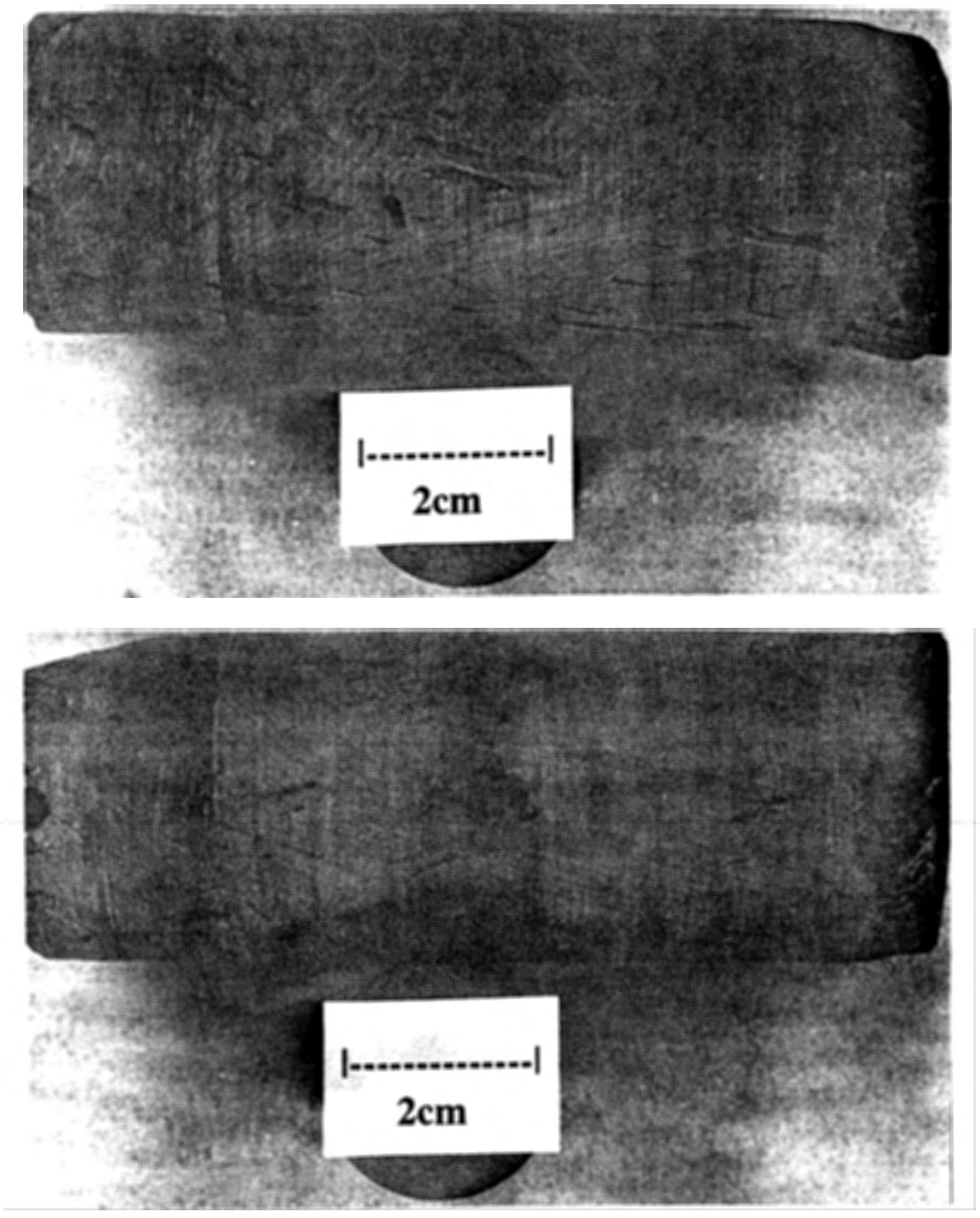

Figure 2B Sample BH-20-2.1 (top) and BH-20-2.1 (bottom).

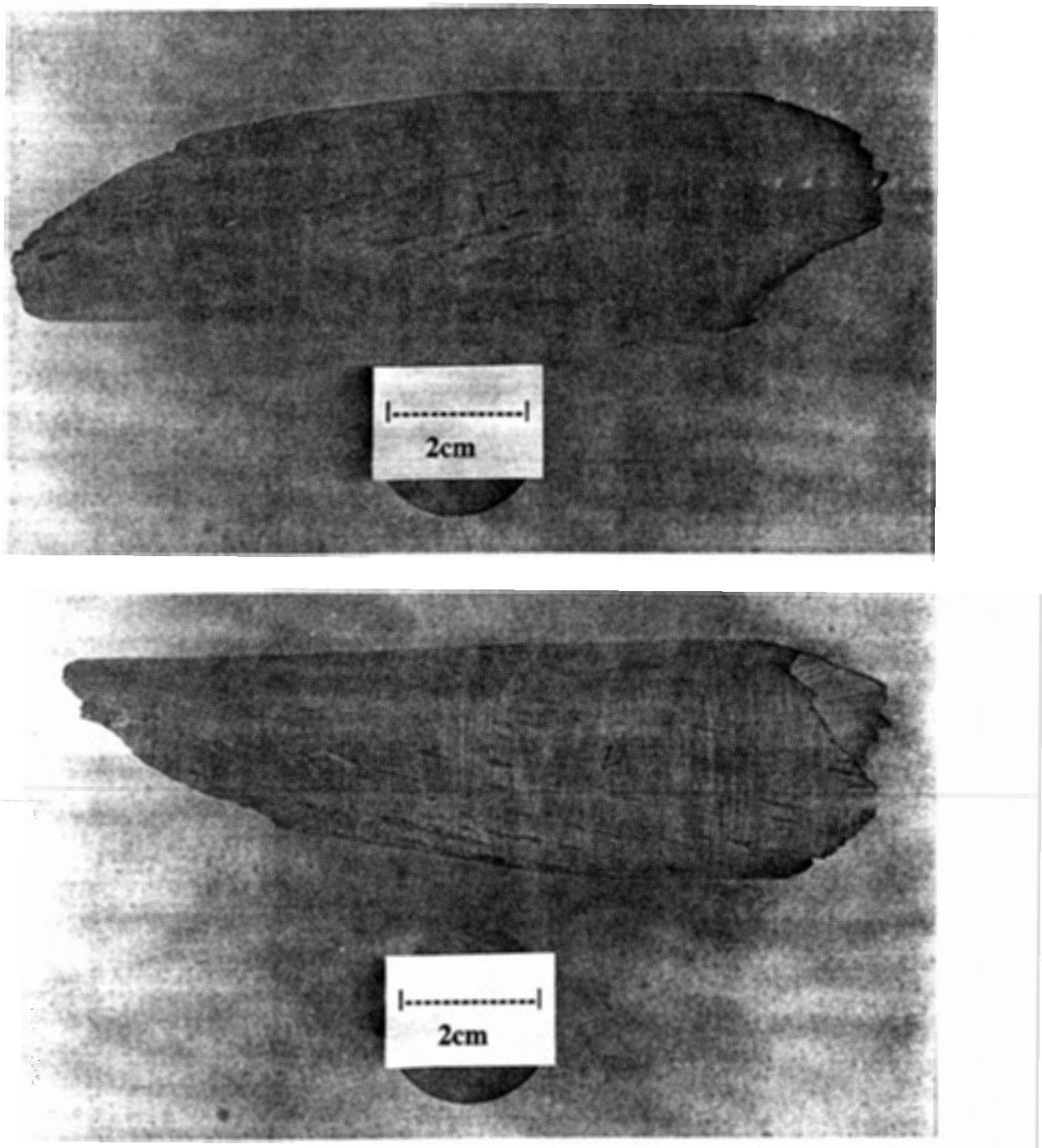

Figure 3B Sample BH-20-4.1 (top) and BH-20-4.2 (bottom).

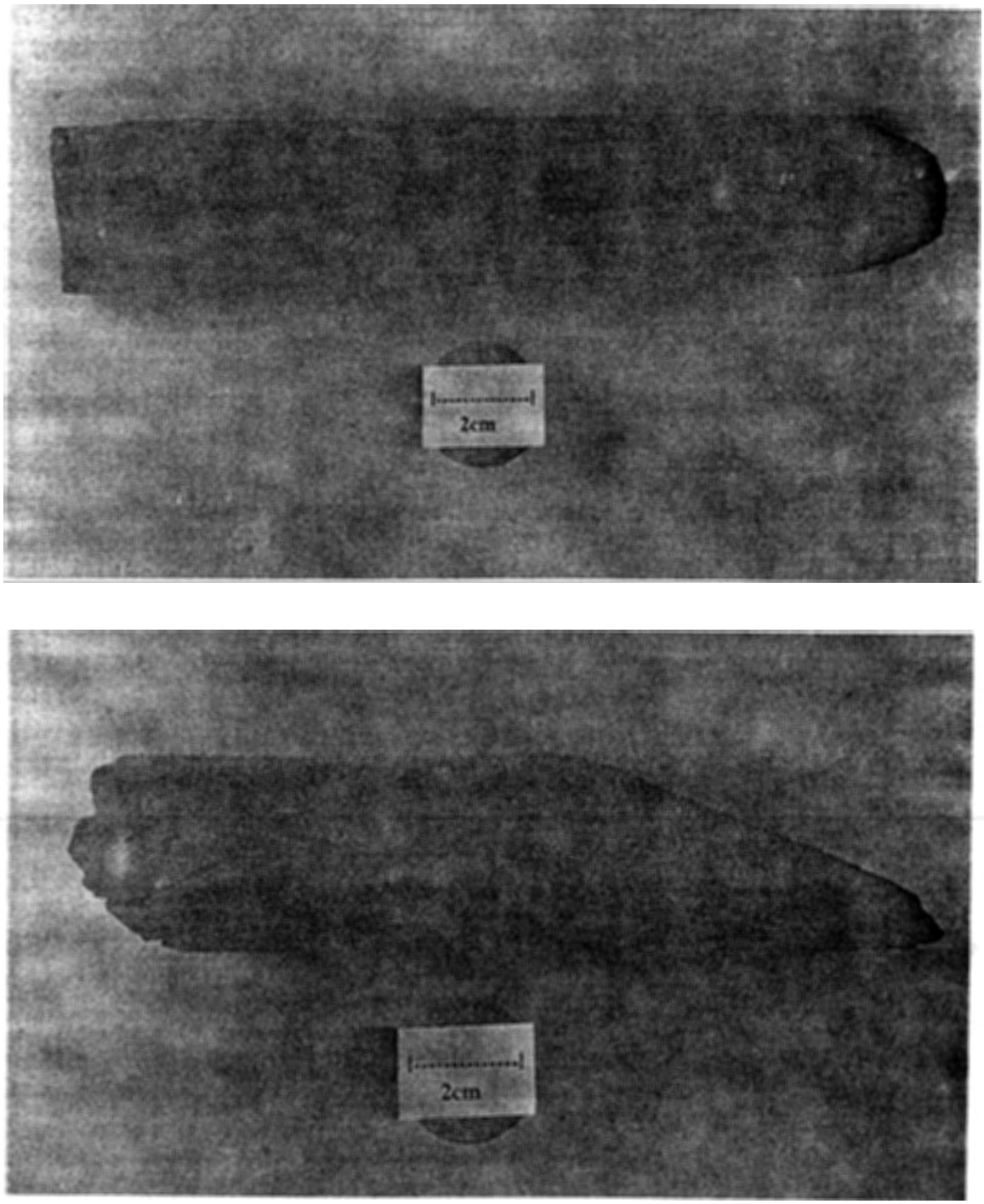

Figure 4B Sample BH-16-1 (top) and BH-8-1 (bottom).

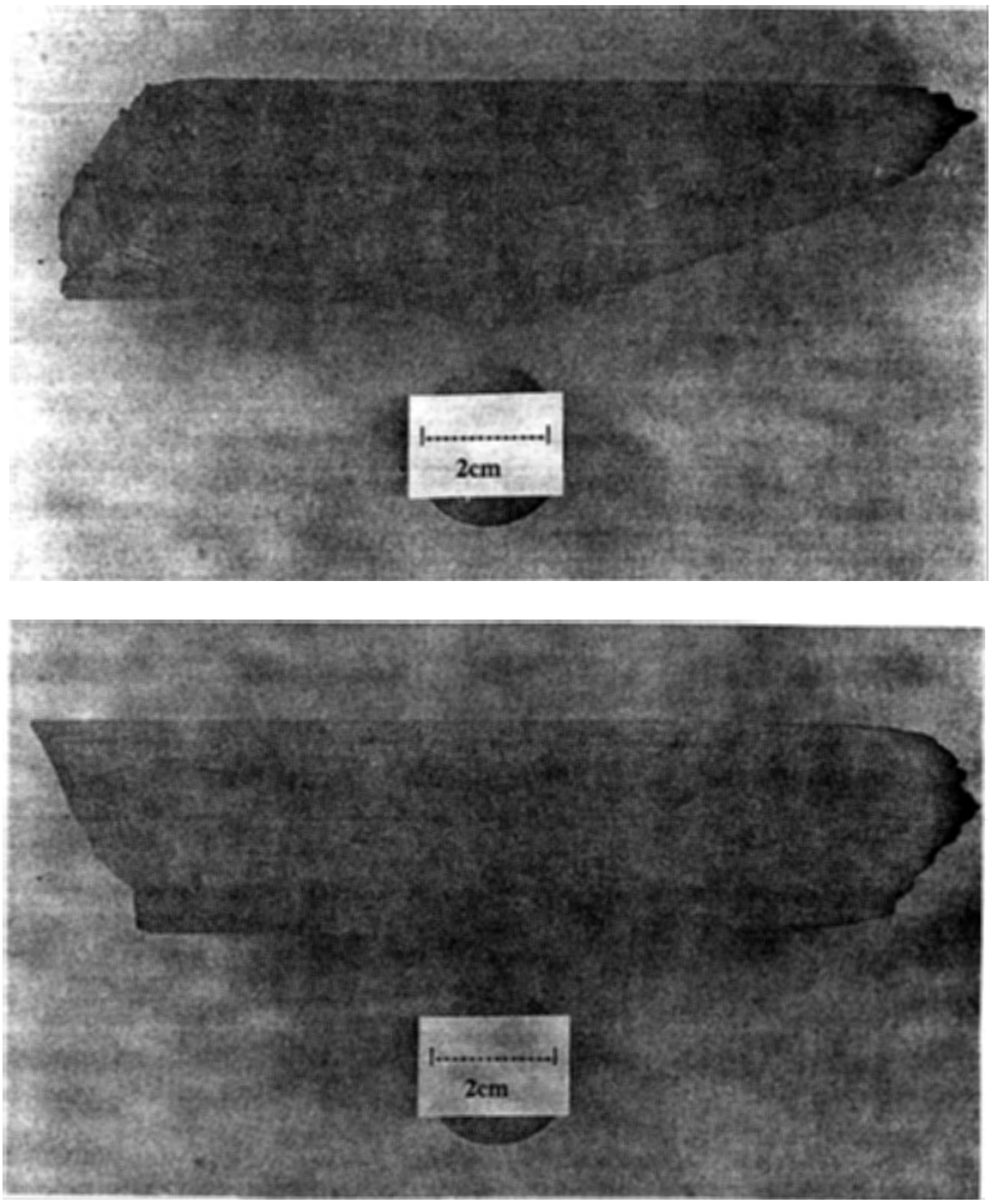

Figure 5B Sample BH-8-2 (top) and BH-8-3 (bottom).

Appendix C

Selected Microprobe analyses with CorrespondingPhotomicrograph Figures

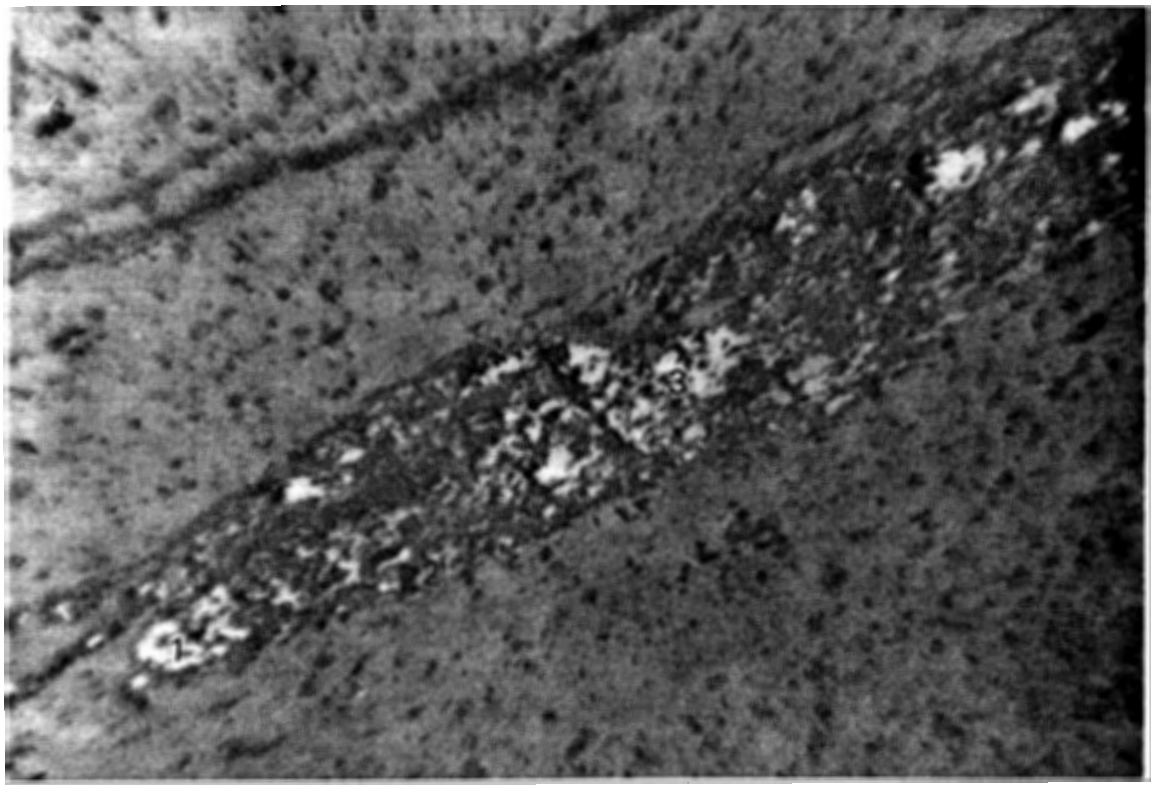

Figure 1C. **Sample HIAC-23.** Reflected light. Pyrrhotite (bronze) replaced by pyrite (white/gold) with small amounts of covellite (indigo blue) (f.o.v. 5.75 mm).

Location		1	2	3	4
Atomic %	Fe	46.713	33.668	47.159	33.594
	S	52.929	65.723	52.696	66.078
	As	0	0	0	0.181
	Si	0	0.126	0	0
Total		99.642	99.517	99.855	100.00
Element %	Fe	60.227	46.412	60.184	46.347
	S	39.173	52.008	38.604	52.331
	As	0.300	0.303	0	0.336
	Si	0.119	0.126	0	0
Total		99.819	99.231	98.788	99.014
Mineral Name		pyrrhotite	pyrite	pyrrhotite	pyrite

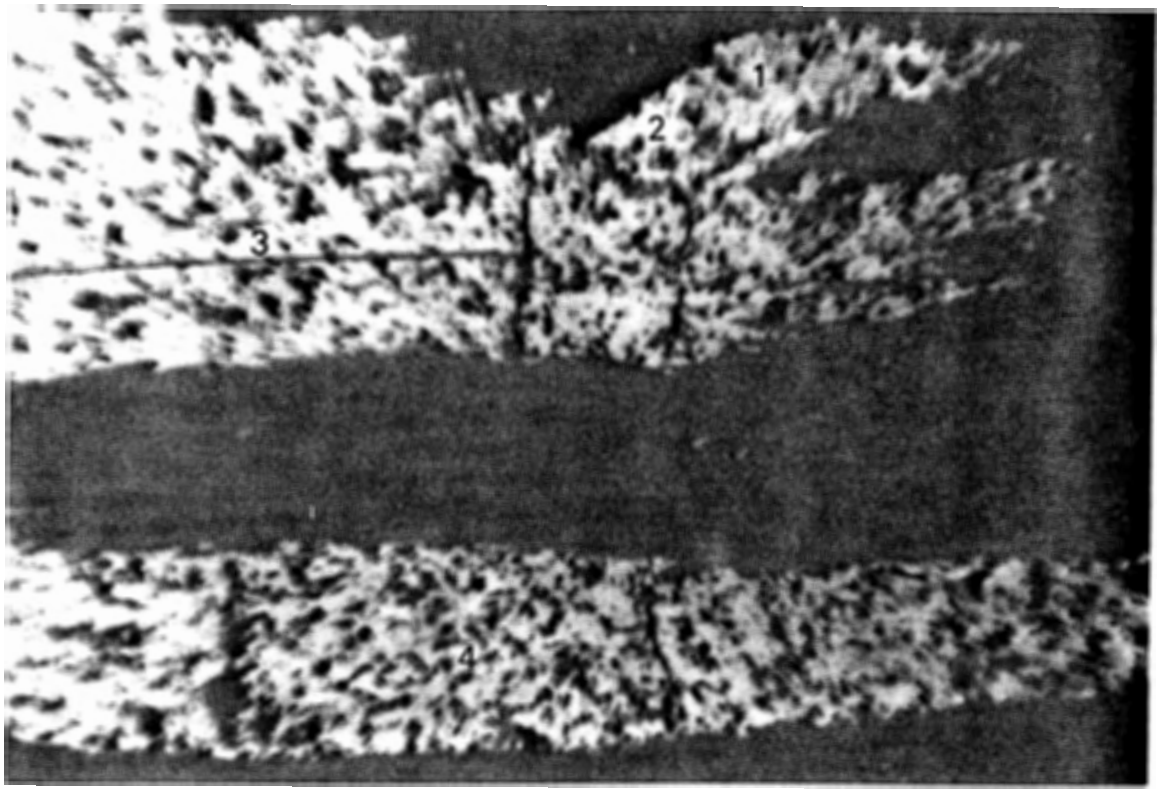

Figure 2C. **Sample HIAC-50.** Reflected light. Pyrrhotite (taupe) with chalcopyrite (dark gold) (f.o.v. 5.75 mm).

Location		1	2	3	4
Atomic %	**Fe**	25.453	46.567	46.638	46.705
	S	49.608	53.150	53.260	53.089
	Cu	24.939	0	0	0
Total		100.00	99.717	99.898	99.794
Element %	**Fe**	30.871	60.177	60.062	60.045
	S	34.538	39.427	39.373	39.180
	Cu	34.412	0	0	0
Total		99.820	99.604	99.435	99.225
Mineral Name		chalcopyrite	pyrrhotite	pyrrhotite	pyrrhotite

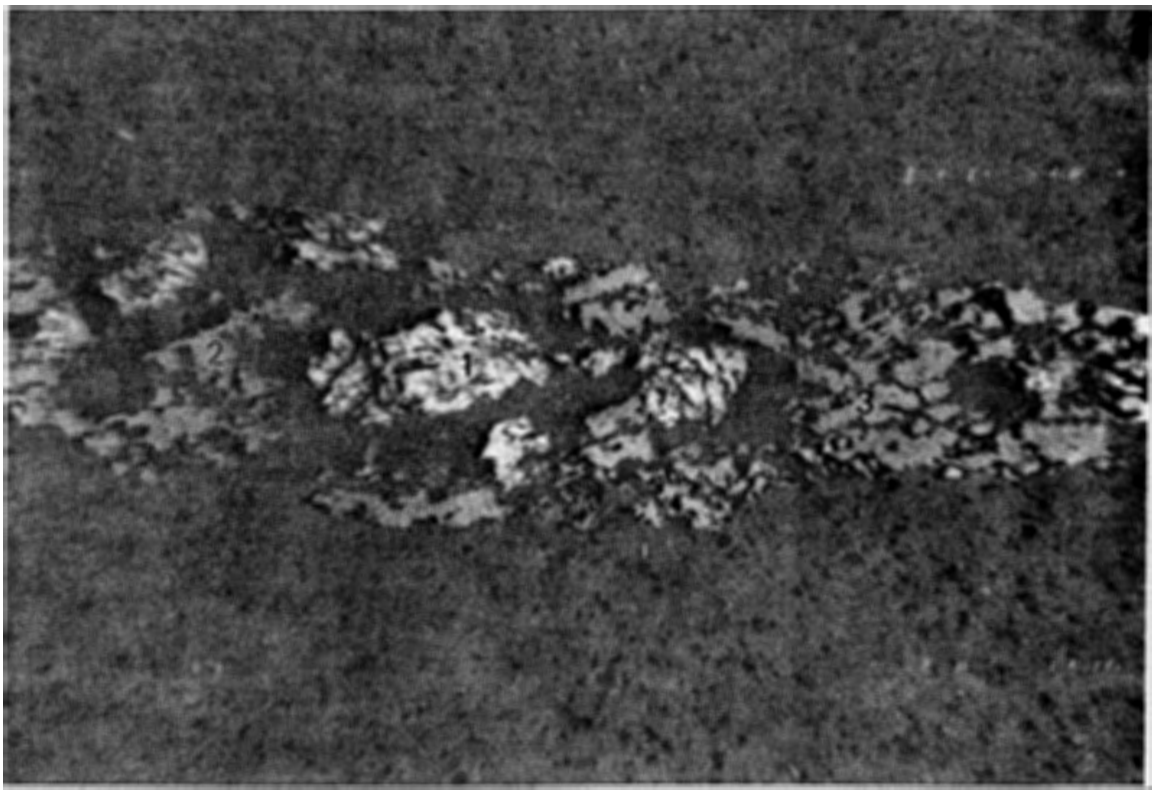

Figure 3C. **Sample HIAC-53.** Reflected light. Pyrrhotite (taupe) with pyrite (white/gold) inclusions (f.o.v. 5.75 mm).

Location		1	2	3
Atomic %	Fe	33.260	46.553	46.495
	S	66.627	53.168	53.313
	As	0	0.151	0
Total		99.887	99.872	99.808
Element %	Fe	46.890	60.212	60.401
	S	53.920	39.475	39.756
	As	0	0.261	0
Total		100.81	99.948	100.157
Mineral Name		pyrite	pyrrhotite	pyrrhotite

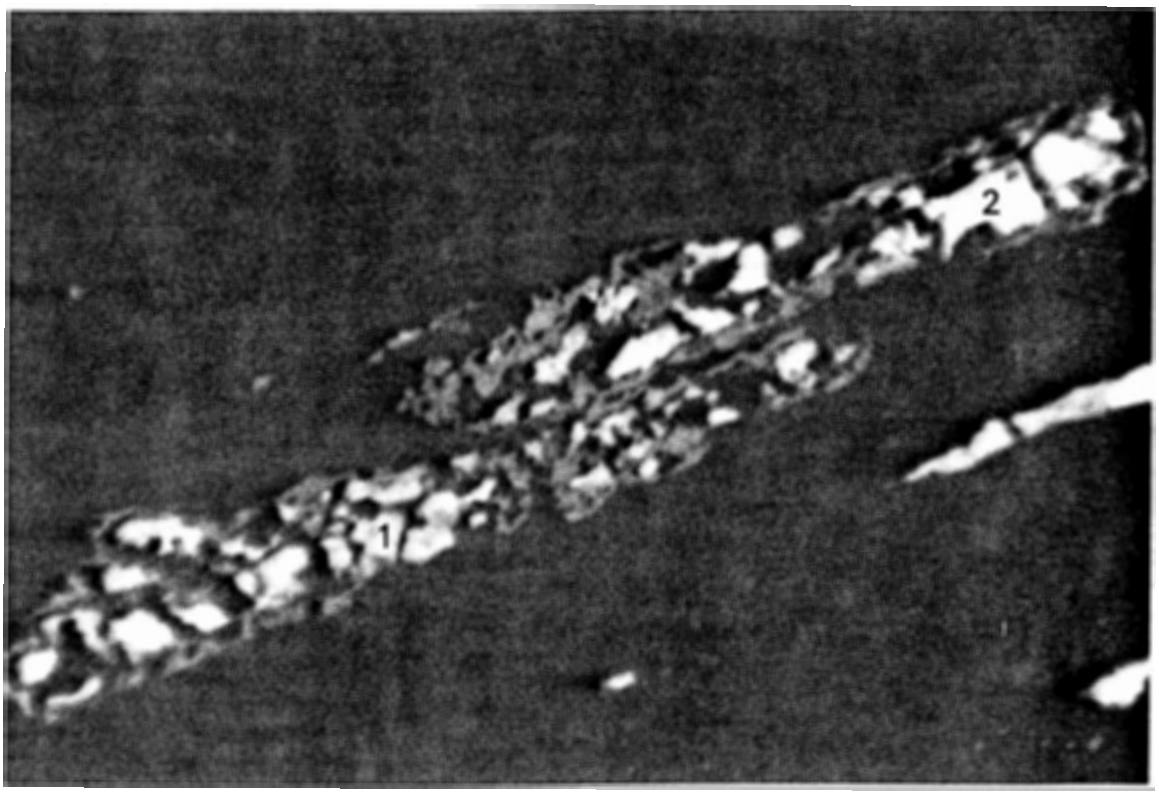

Figure 4C. **Sample HIAC-54.** Reflected light. Elongate pyrrhotite (pale bronze) grains surrounded by rutile (light grey) (f.o.v. 5.75 mm).

Location		1	2
Atomic %	Fe	46.828	46.306
	S	52.871	53.152
	As	0	0
	Al	0	0.212
	Si	0	0.188
Total		99.699	99.858
Element %	Fe	60.999	59.347
	S	39.534	39.104
	As	0	0
	Al	0	0.131
	Si	0	0.121
Total		100.533	98.695
Mineral Name		pyrrhotite	pyrrhotite

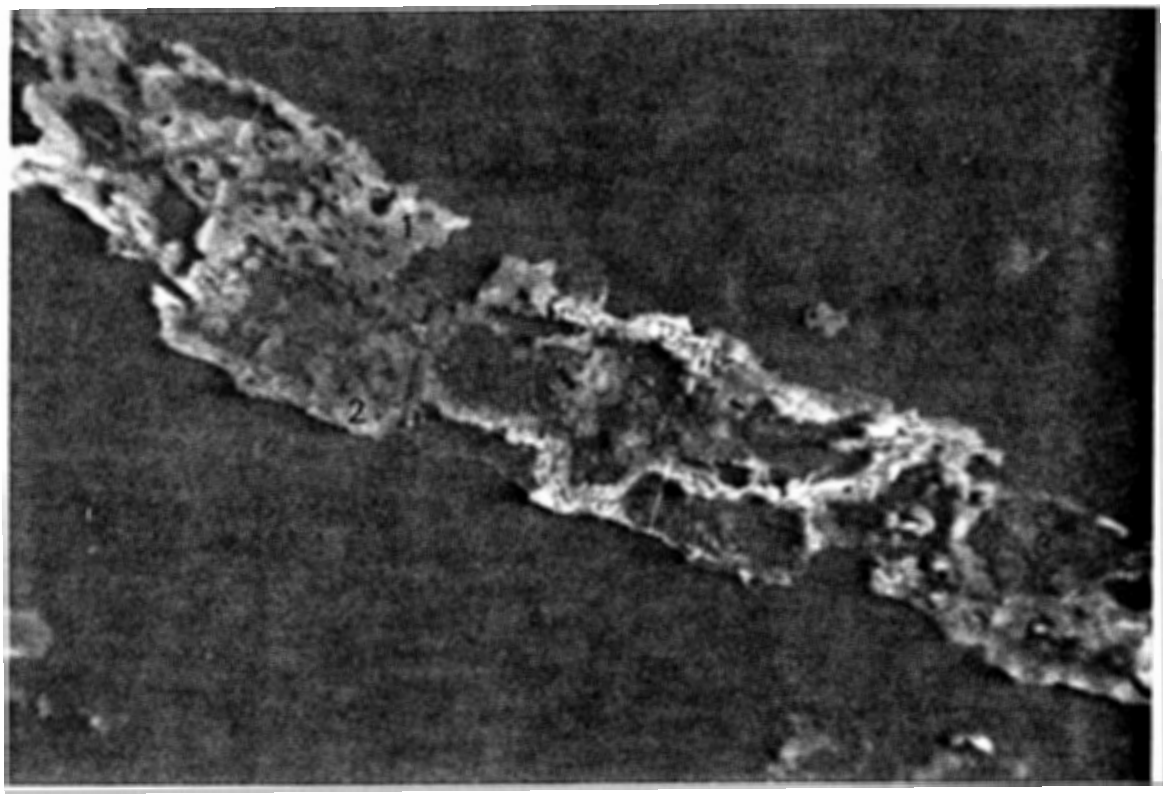

Figure 5C. Sample HIAC-56. Reflected light. Highly altered and tarnished pyrite (f.o.v 5.75 mm).

Location		1	2	3
Atomic %	**Fe**	34.379	33.663	34.133
	S	65.526	66.054	65.570
	As	0	0.130	0.146
Total		99.905	99.847	99.849
Element %	**Fe**	46.611	46.606	45.962
	S	50.997	52.497	50.683
	As	0	0.242	0.265
Total		97.608	99.345	96.910
Mineral Name		pyrite	pyrite	pyrite

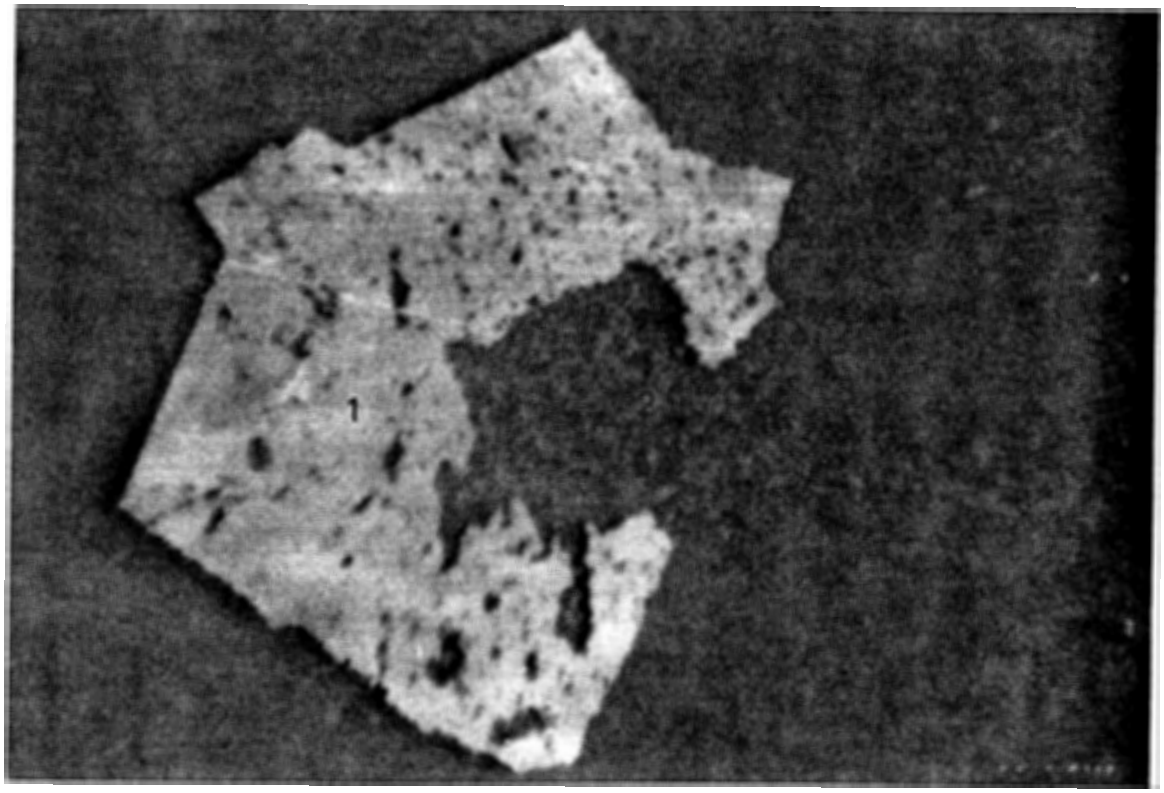

Figure 6C. Sample HIAC-57. Reflected light. Arsenopyrite crystals with pyrrhotite (dark bronze) inclusion (f.o.v. 5.75 mm).

Location		1	2
Atomic %	Fe	33.405	44.781
	S	34.198	51.480
	As	32.147	0.183
	Si	0.250	1.555
	Al	0	1.733
Total		100.00	99.732
Element %	Fe	34.851	58.476
	S	20.480	38.589
	As	44.990	0.320
	Si	0.131	1.021
	Al	0	1.093
Total		100.452	99.498
Mineral Name		arsenopyrite	pyrrhotite

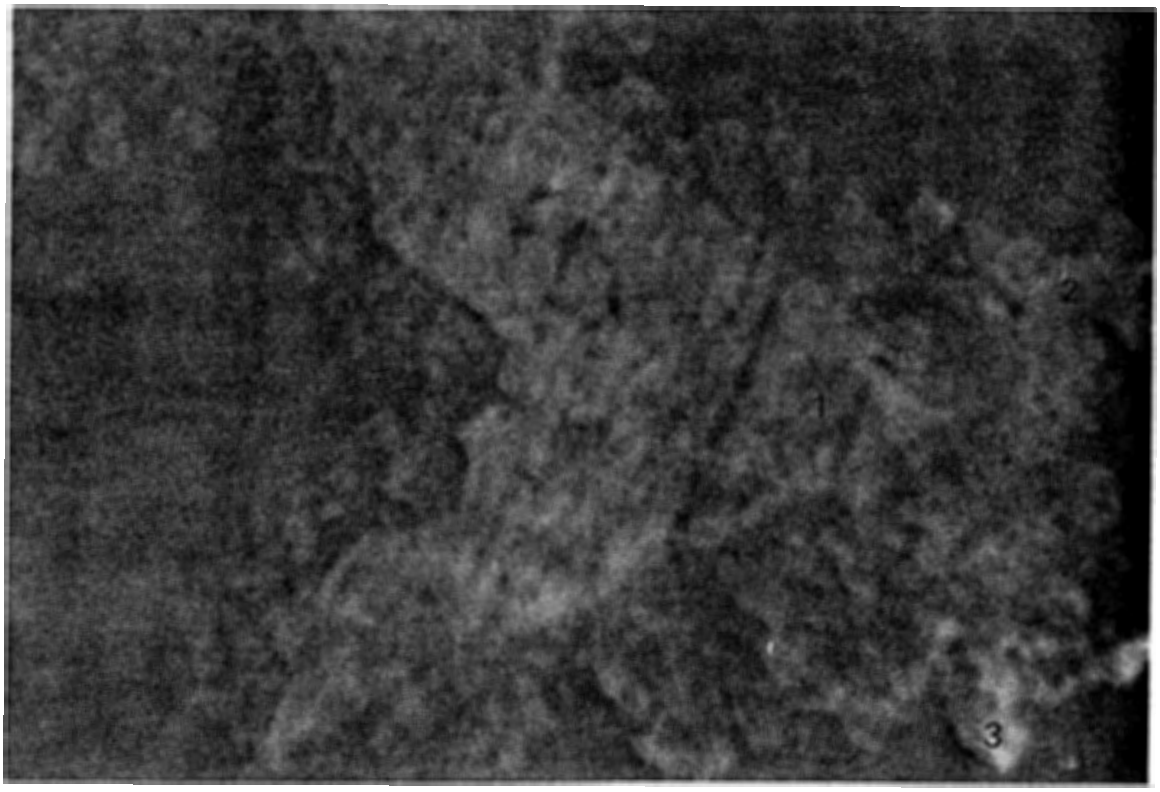

Figure 7C. **Sample HIAC-59.** Reflected light. Altered pyrite crystal (f.o.v. 5.75 mm).

Location		1	2	3
Atomic %	Fe	33.155	33.242	33.025
	S	66.157	66.132	66.507
	As	0.170	0	0
	Al	0.218	0	0
	Si	0.245	0.402	0.374
Total		99.946	99.777	99.906
Element %	Fe	46.488	46.993	46.565
	S	53.248	53.665	53.829
	As	0.320	0	0.178
	Al	0.148	0	0
	Si	0.173	0.286	0.265
Total		100.377	100.944	100.659
Mineral Name		pyrite	pyrite	pyrite

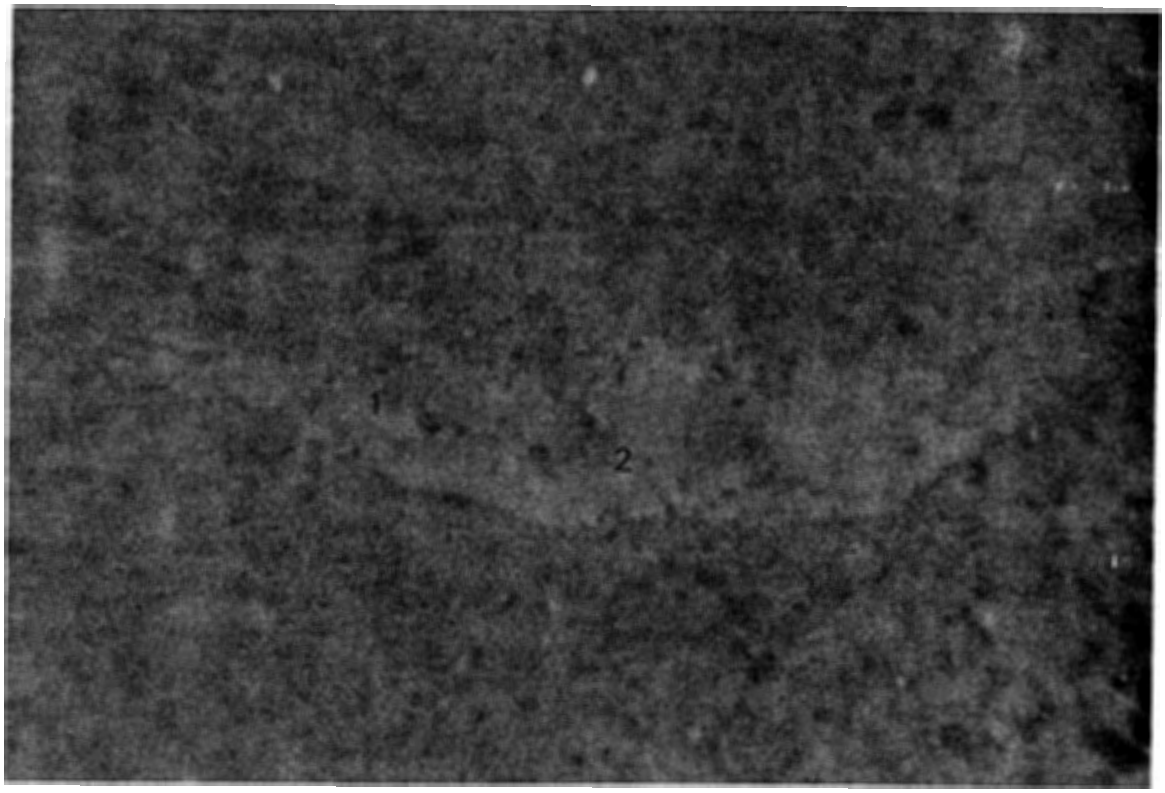

Figure 8C. **Sample BH-8-1.** Reflected light. Pyrrhotite (bronze) rimmed by pyrite (gold) (f.o.v. 5.75 mm).

Location		1	2	3
Atomic %	**Fe**	46.965	33.609	46.459
	S	52.832	66.198	53.161
	Co	0	0	0.270
	W	0	0.087	0
Total		99.797	99.894	99.890
Element %	**Fe**	60.892	46.470	59.893
	S	39.321	52.541	39.340
	Co	0	0	0.368
	W	0	0.634	0
Total		100.213	99.645	99.601
Mineral Name		pyrrhotite	pyrite	pyrrhotite

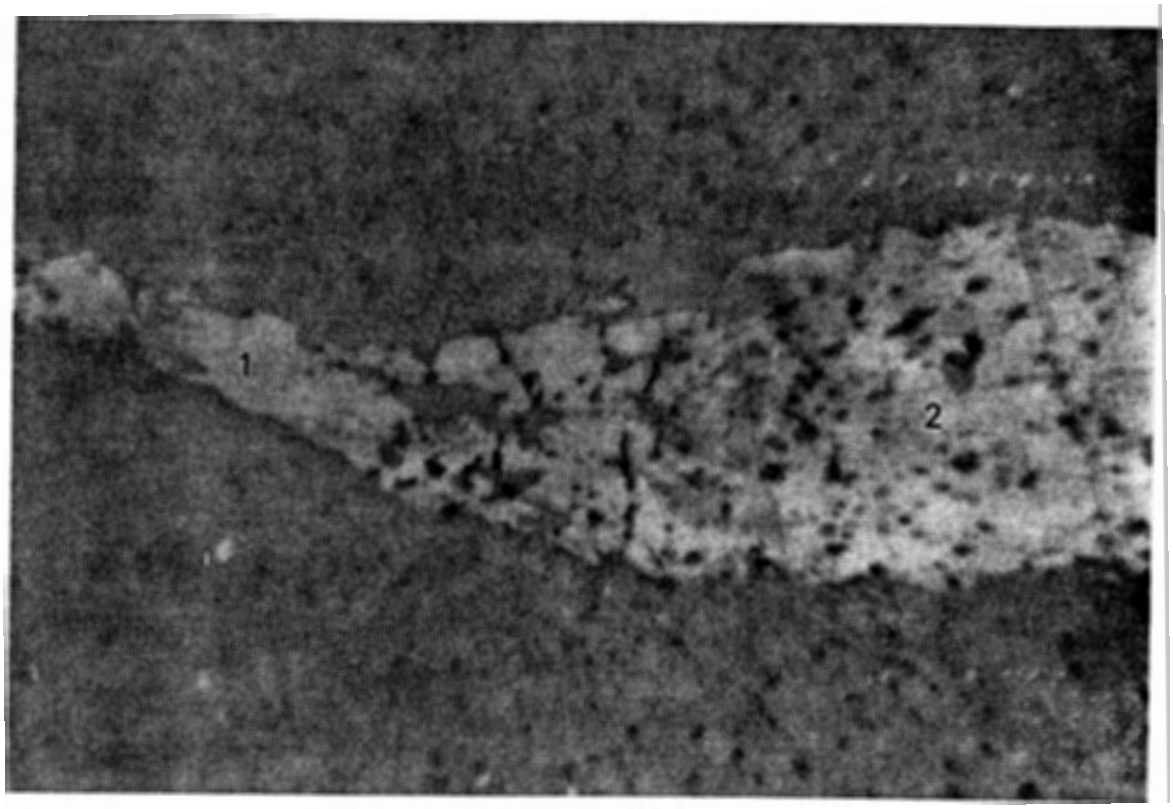

Figure 9C. Sample BH-8-1. Reflected light. Elongate pyrrhotite (f.o.v. 5.75 mm).

Location		1	2
Atomic %	Fe	46.181	46.476
	S	53.692	53.362
	As	0	0.162
Total		99.873	100.00
Element %	Fe	59.275	60.051
	S	39.560	39.578
	As	0	0.281
Total		98.835	99.910
Mineral Name		pyrrhotite	pyrrhotite

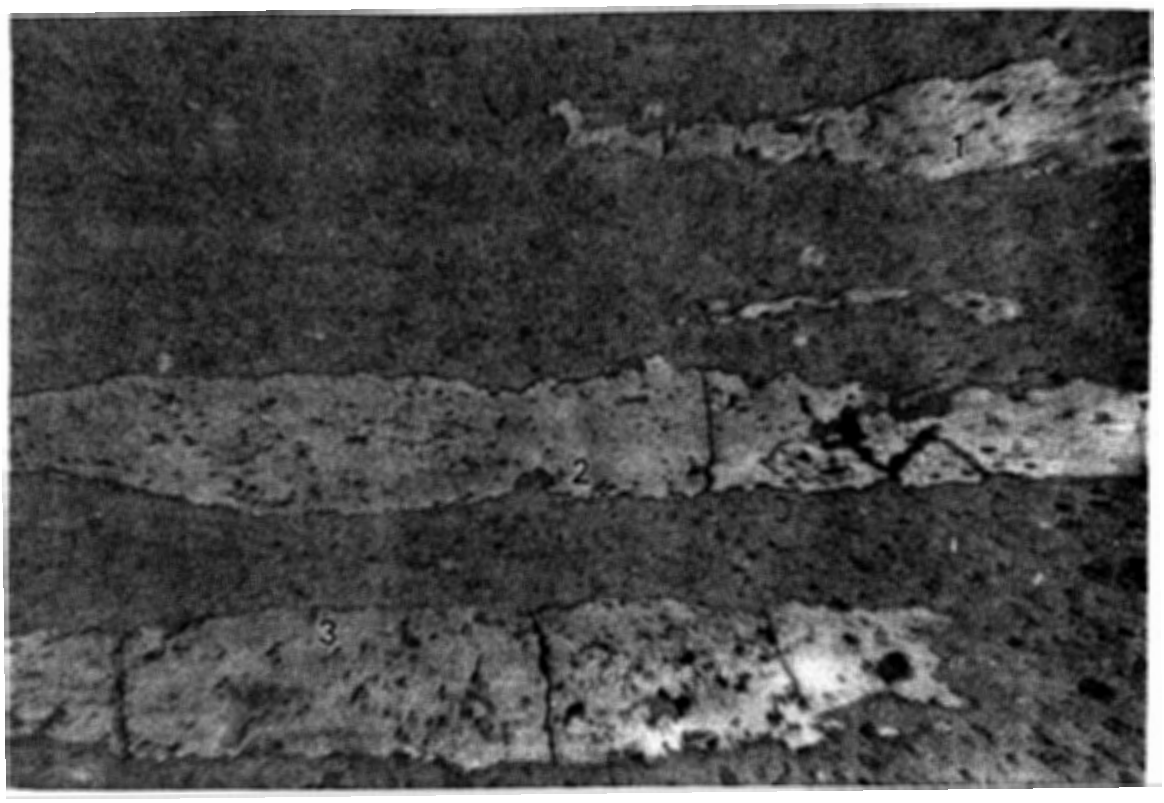

Figure 10 C. Sample BH-8-2. Reflected light. Elongate pyrrhotite running parallel to cleavage (f.o.v. 5.75 mm).

Location		1	2	3
Atomic %	**Fe**	46.969	46.817	46.636
	S	52.921	53.021	53.042
	As	0	0.162	0
Total		99.890	100.00	99.678
Element %	**Fe**	61.140	61.154	61.189
	S	39.545	39.757	39.950
	As	0	0.284	0
Total		100.685	101.194	101.733
Mineral Name		pyrrhotite	pyrrhotite	pyrrhotite

Same as BH-8-1 ?? Pg C-10 !

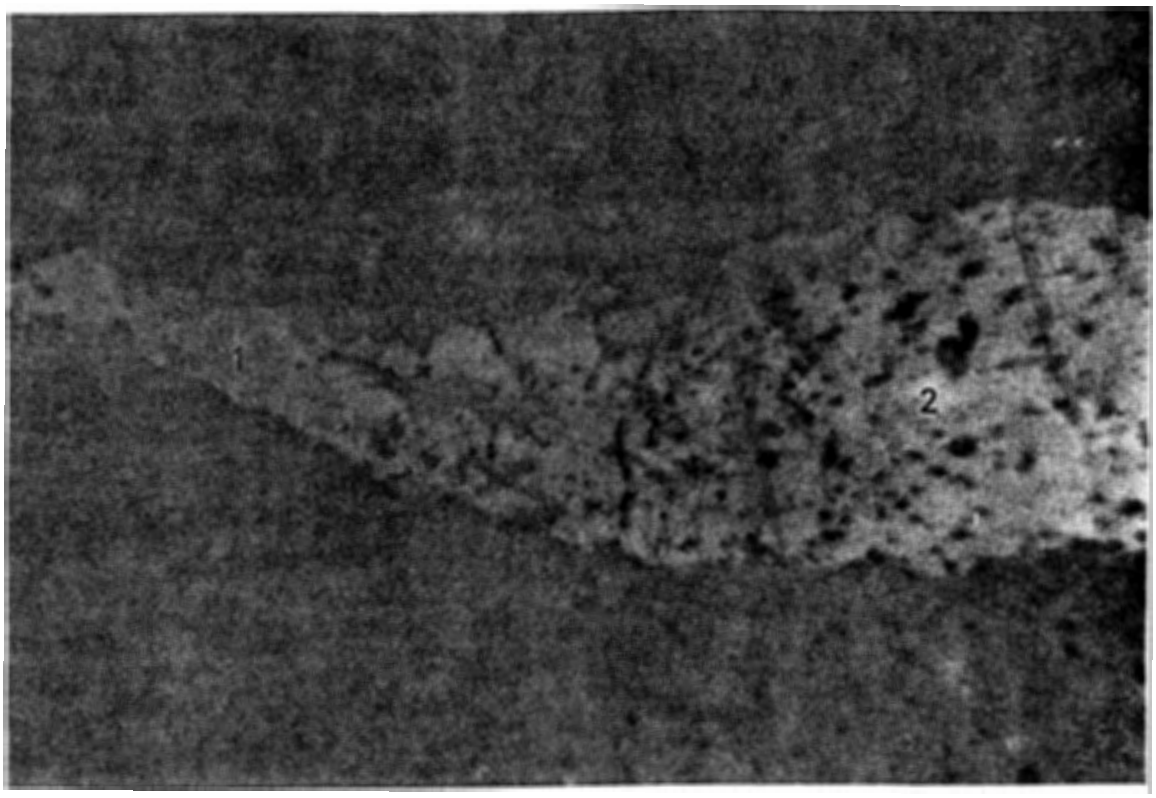

Figure 11C. Sample BH-8-3. Reflected light. [Rotated pyrrhotite porphyroclast] ? (f.o.v. 5.75 mm).

Location		1	2
Atomic %	**Fe**	46.532	46.664
	S	53.287	52.985
	As	0	0.200
Total		99.819	99.849
Element %	**Fe**	59.931	60.229
	S	39.397	39.257
	As	0	0.346
Total		99.328	99.832
Mineral Name		pyrrhotite	pyrrhotite

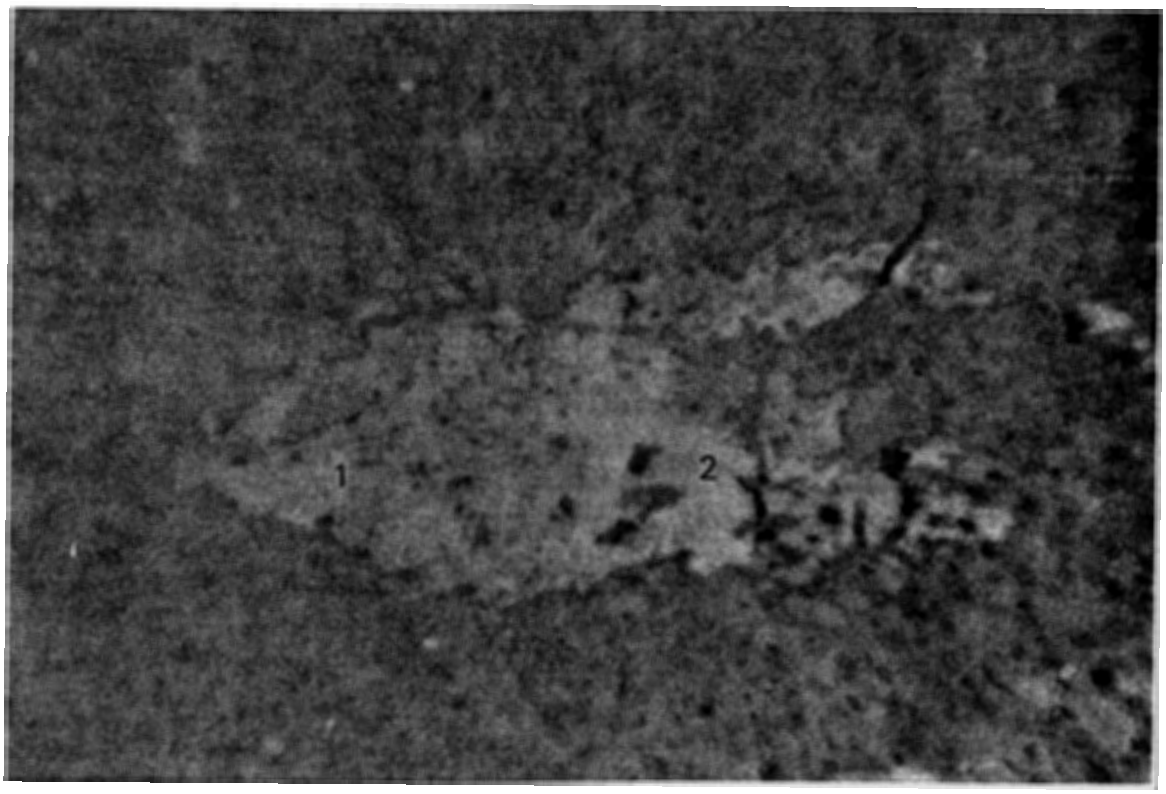

Figure 12C. Sample BH-8-3. Reflected light. Pyrrhotite grain (f.o.v. 5.75 mm).

Location		1	2
Atomic %	**Fe**	46.757	46.367
	S	53.076	53.330
	As	0	0.159
Total		99.833	99.856
Element %	**Fe**	60.245	59.500
	S	39.256	39.284
	As	0	0.274
Total		99.501	99.058
Mineral Name		pyrrhotite	pyrrhotite

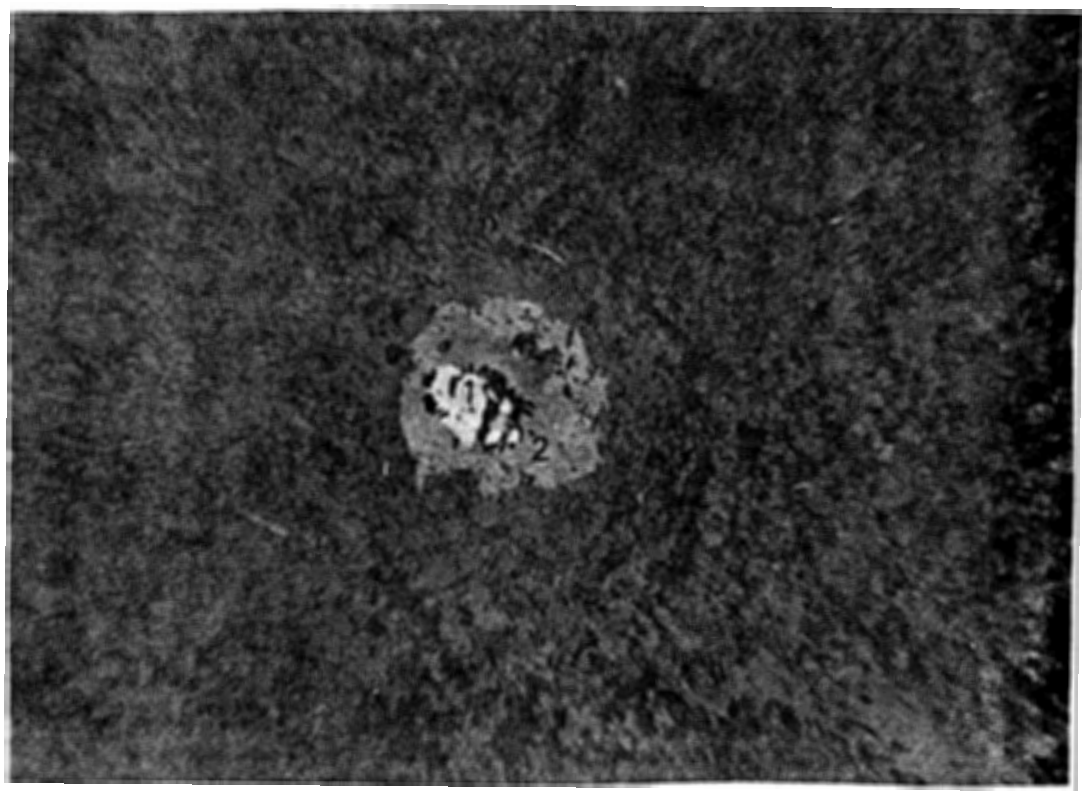

Figure 13C. Sample BH-16-1. Reflected light. Pyrite (white/gold) rimmed by pyrrhotite (bronze) which is in turn rimmed by rutile (light grey) (f.o.v. 3 mm).

Location		1	2
Atomic %	**Fe**	33.303	44.994
	S	66.477	54.867
Total		99.780	99.861
Element %	**Fe**	46.508	58.367
	S	53.292	40.857
Total		99.800	99.224
Mineral Name		pyrite	pyrrhotite

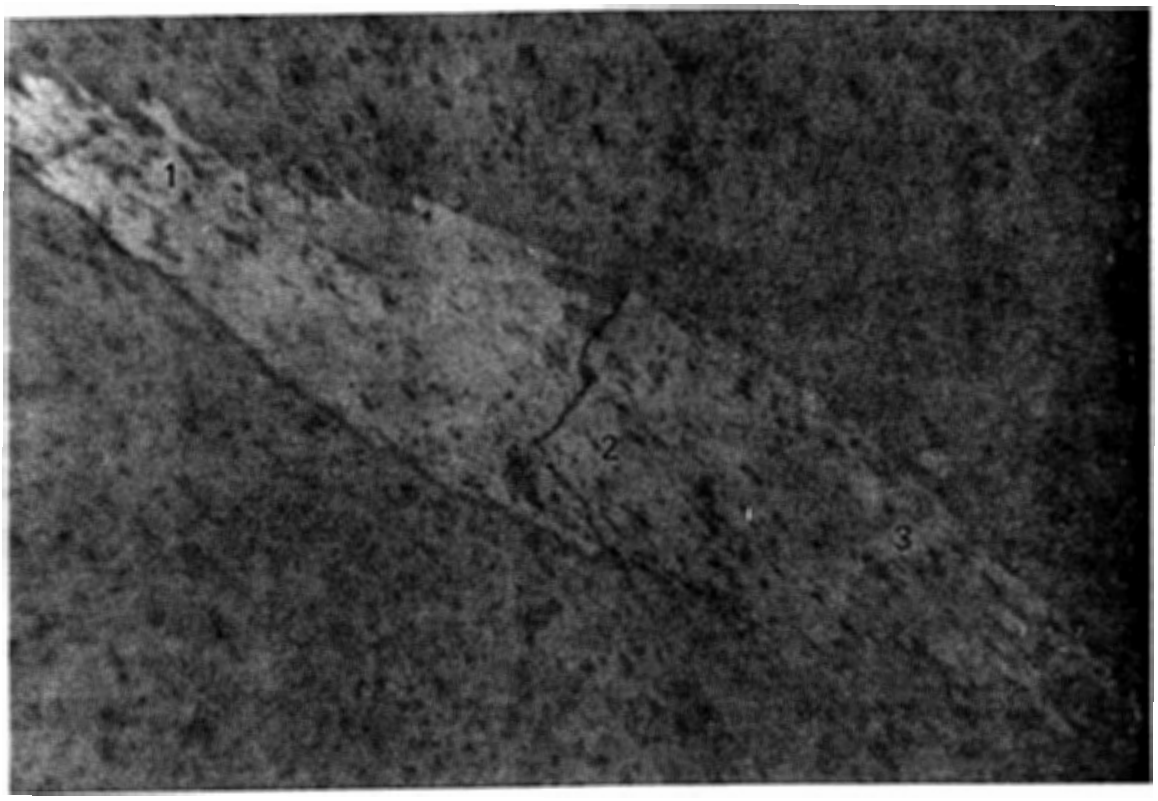

Figure 14C. Sample BH-20-1.1. Reflected light. Pyrrhotite grain (f.o.v. 5.75 mm).

Location		1	2	3
Atomic %	**Fe**	46.681	46.573	46.794
	S	53.018	53.085	53.003
	Si	0.187	0.199	0
Total		99.886	99.857	99.797
Element %	**Fe**	59.828	60.324	60.281
	S	39.006	39.471	39.195
	Si	0.121	0.130	0
Total		98.955	99.925	99.476
Mineral Name		pyrrhotite	pyrrhotite	pyrrhotite

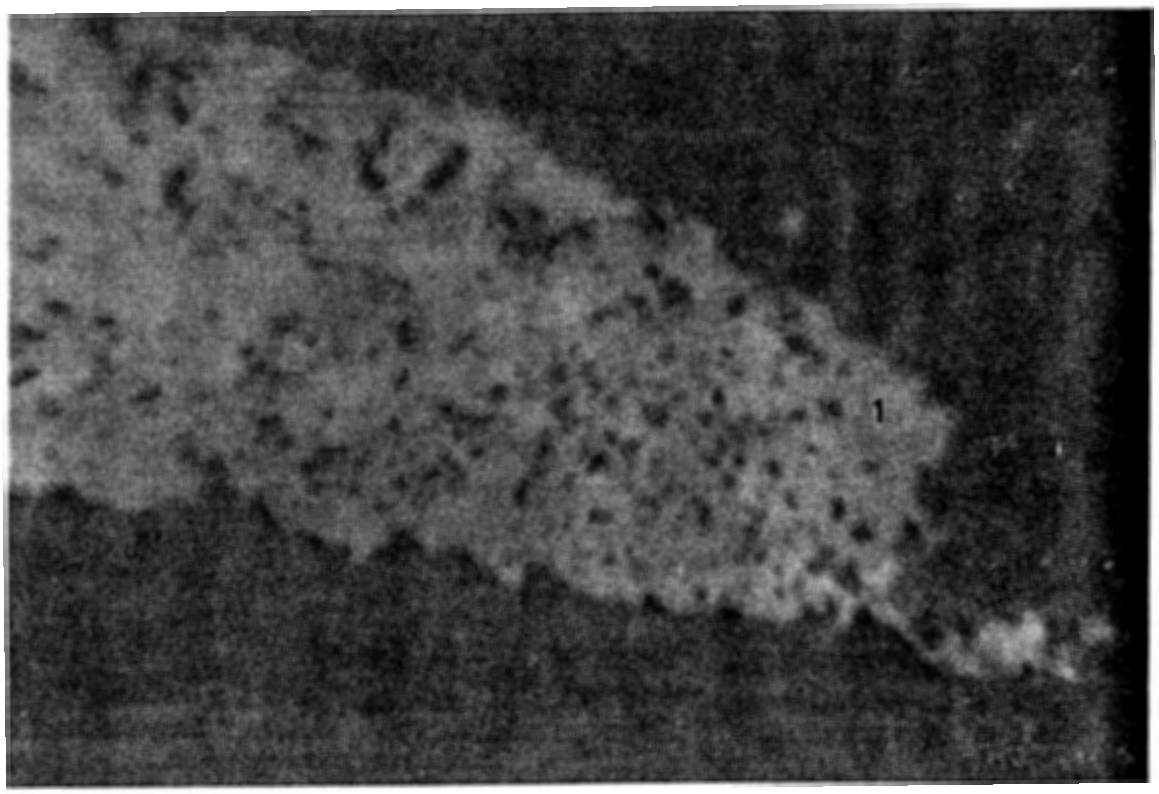

Figure 15C. Sample BH-20-1.2. Reflected light. Pyrite porphyroblast (white/gold) with chalcopyrite (dark gold) (f.o.v. 5.75 mm).

Location		1	2
Atomic %	**Fe**	33.892	25.163
	S	65.980	49.757
	Cu	0	25.080
Total		99.872	100.00
Element %	**Fe**	46.793	30.194
	S	52.291	34.274
	Cu	0	34.239
Total		99.084	98.706
Mineral Name		pyrite	chalcopyrite

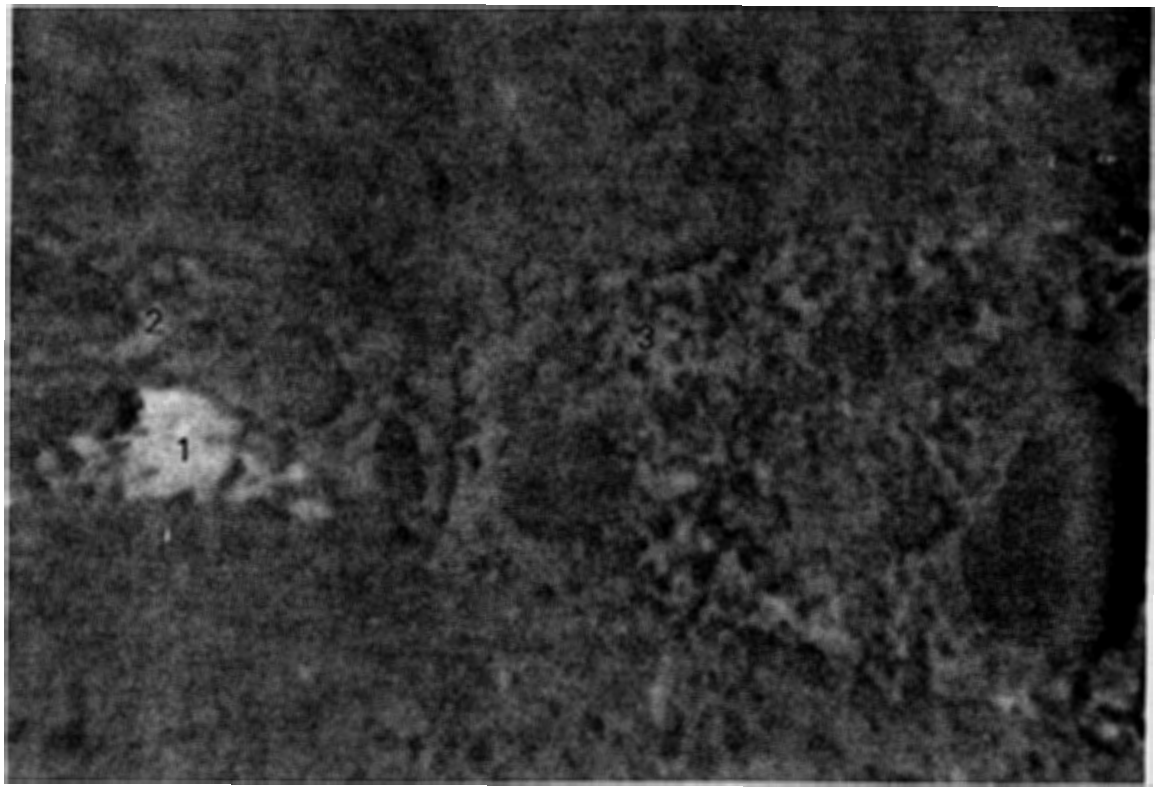

Figure 16C. Sample BH-20-1.2. Reflected light. Pyrrhotite (taupe) and pyrite (white/gold) with abundant inclusions of the host rock (slate) and opaques (f.o.v. 5.75 mm).

Location		1	2	3
Atomic %	Fe	33.660	44.891	45.142
	S	65.987	55.010	54.710
	As	0	0	0.148
Total		99.647	99.901	100.00
Element %	Fe	46.600	58.119	58.562
	S	52.441	40.882	40.743
	As	0	0	0.258
Total		99.041	99.001	99.563
Mineral Name		pyrite	pyrrhotite	pyrrhotite

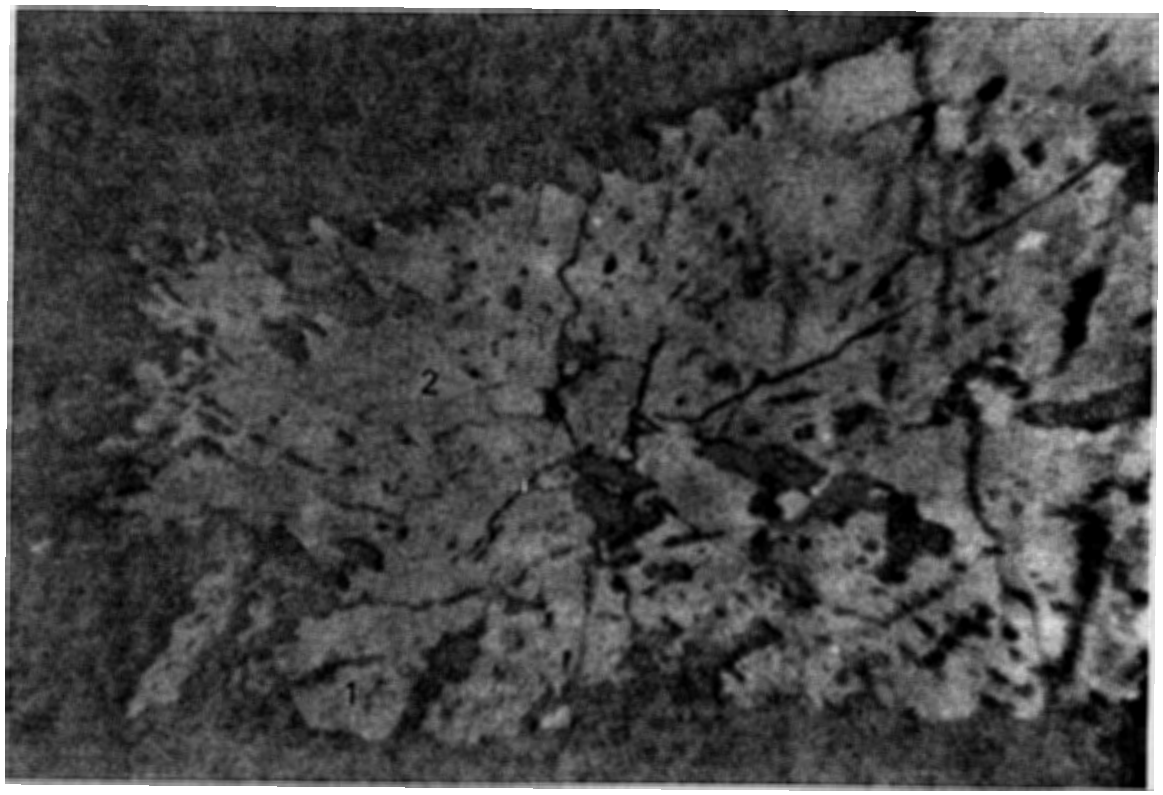

Figure 17C. Sample BH-20-1.3. Reflected light. Pyrrhotite grain (f.o.v. 5.75 mm).

Location		1	2
Atomic %	**Fe**	46.620	46.531
	S	53.105	53.243
Total		99.725	99.774
Element %	**Fe**	59.592	59.846
	S	38.967	39.310
Total		98.559	99.156
Mineral Name		pyrrhotite	pyrrhotite

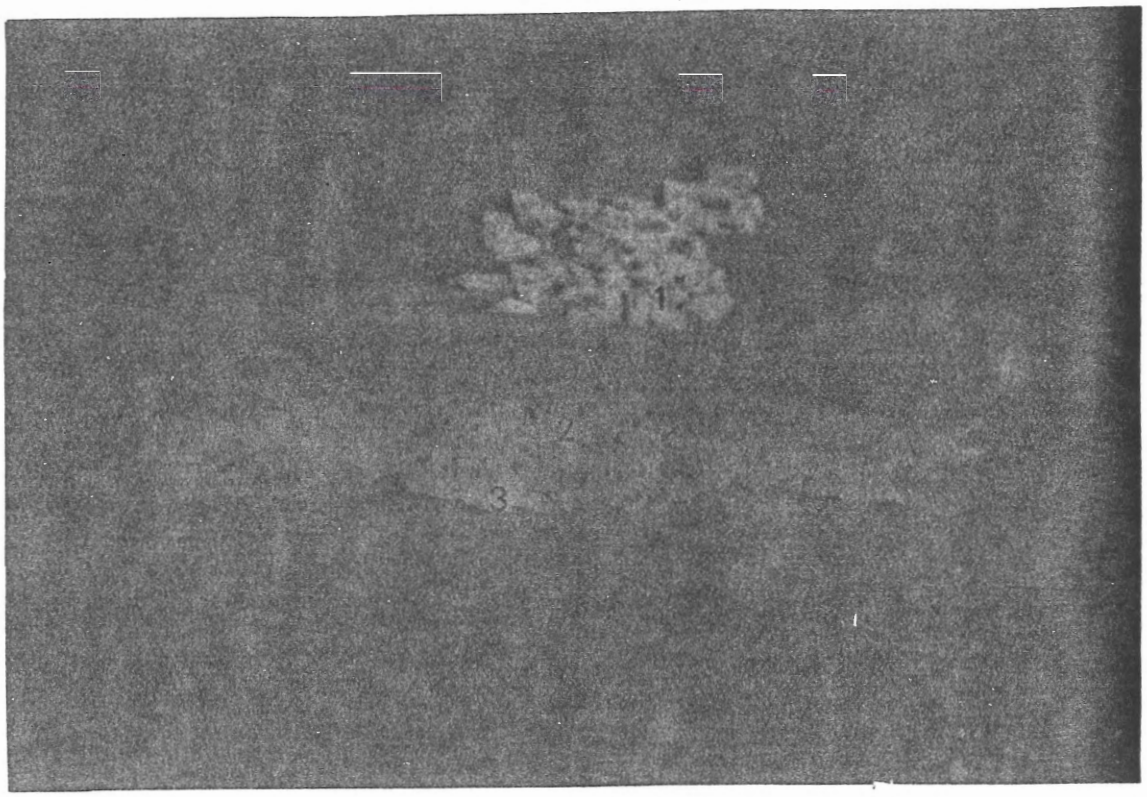

Figure 18C. Sample BH-20-2.1. Reflected light. Pyrite cube (white/gold) and elongate pyrrhotite (bronze) with chalcopyrite (dark gold) (f.o.v. 5.75 mm).

Location		1	2	3
Atomic %	Fe	33.229	46.742	25.488
	S	66.620	53.124	49.750
	As	0.151	0	0
	Cu	0	0	24.627
Total		100.00	99.866	99.865
Element %	Fe	46.937	60.046	31.053
	S	54.020	39.175	34.794
	As	0.286	0	0
	Cu	0	0	34.135
Total		101.243	99.221	99.982
Mineral Name		pyrite	pyrrhotite	chalcopyrite

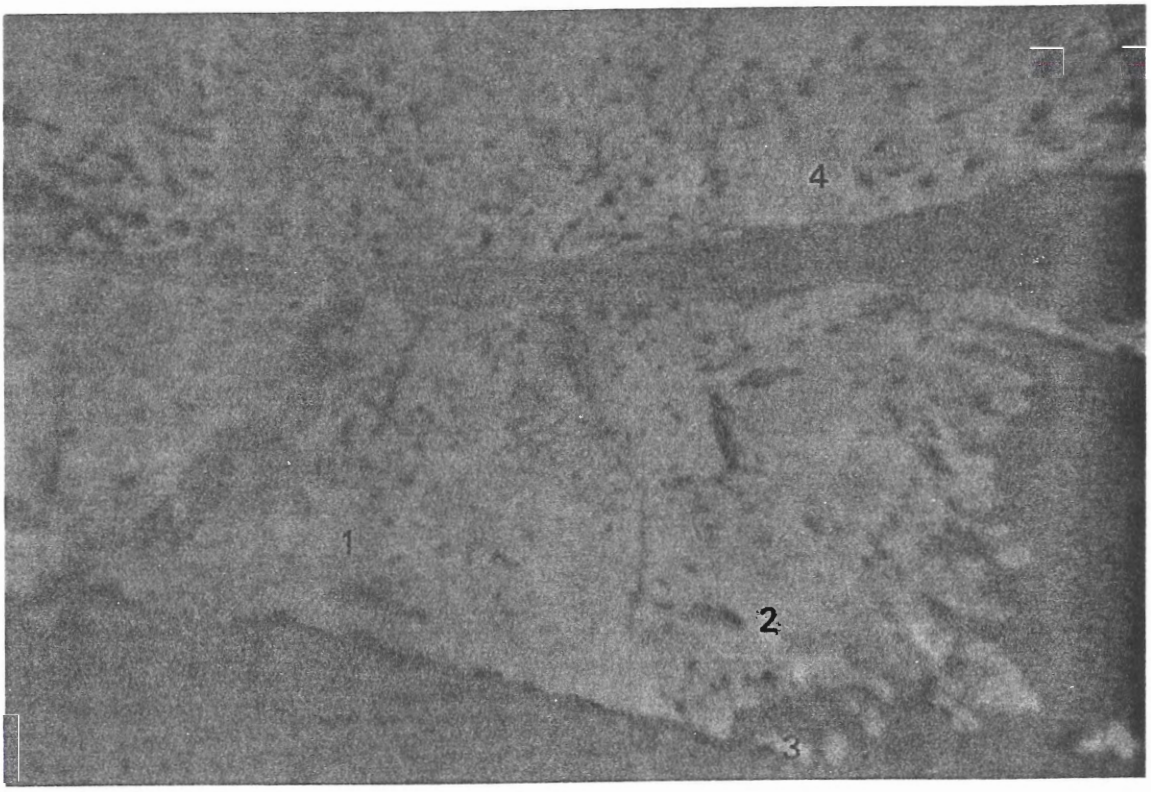

Figure 19C. Sample BH-20-2.1. Reflected light. Pyrrhotite (taupe) with chalcopyrite (dark gold) (f.o.v. 5.75 mm).

Location	1	2	3	4
Atomic % Fe	46.586	46.564	25.450	46.521
S	53.207	53.219	49.876	52.924
As	0.149	0.148	0	0
Cu	0	0	24.675	0
Total	99.942	99.931	100.00	99.445
Element % Fe	60.474	59.903	30.758	60.003
S	39.649	39.301	34.603	39.184
As	0.249	0.255	0	0.249
Cu	0	0	33.928	0
Total	100.372	99.459	99.289	99.908
Mineral Name	pyrrhotite	pyrrhotite	chalcopyrite	pyrrhotite

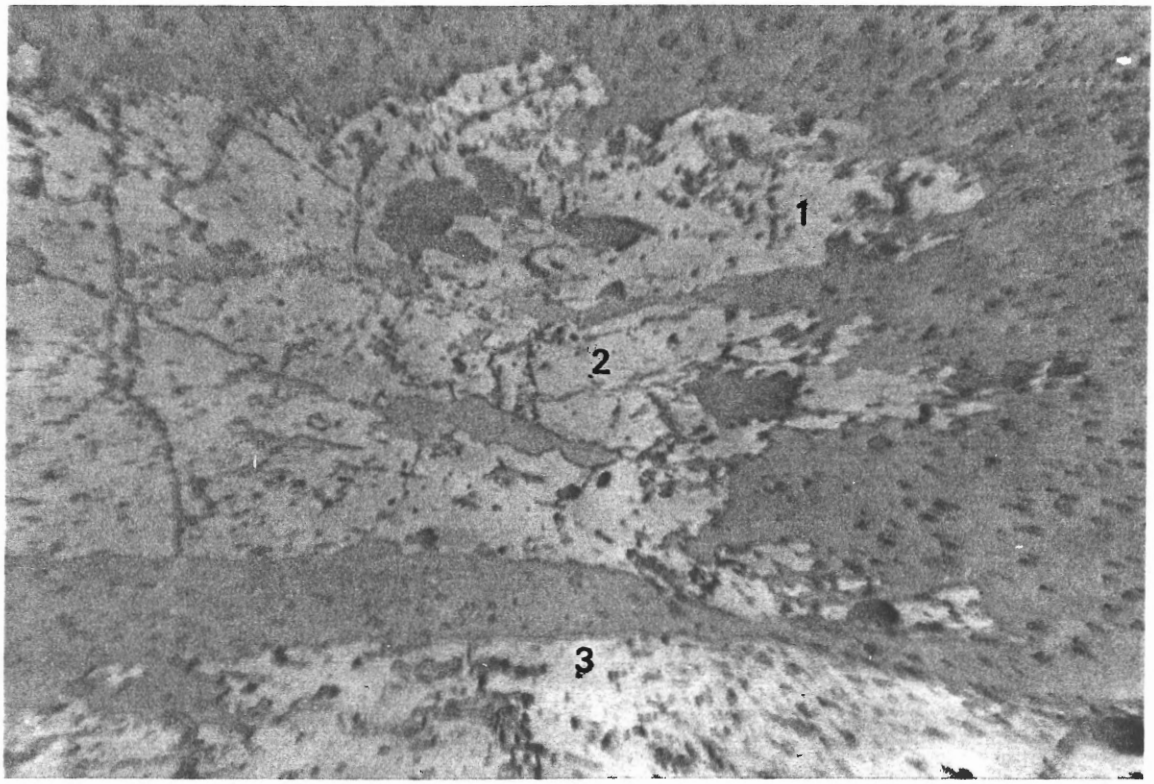

Figure 20C. Sample BH-20-2.2. Reflected light. Pyrrhotite with abundant inclusions of host rock (slate) and opaques (f.o.v. 5.75 mm).

Location		1	2	3
Atomic %	Fe	46.703	46.810	46.538
	S	52.933	53.069	53.349
Total		99.636	99.879	99.887
Element %	Fe	60.577	60.174	60.281
	S	39.411	39.161	39.669
Total		99.988	99.335	99.950
Mineral Number		pyrrhotite	pyrrhotite	pyrrhotite

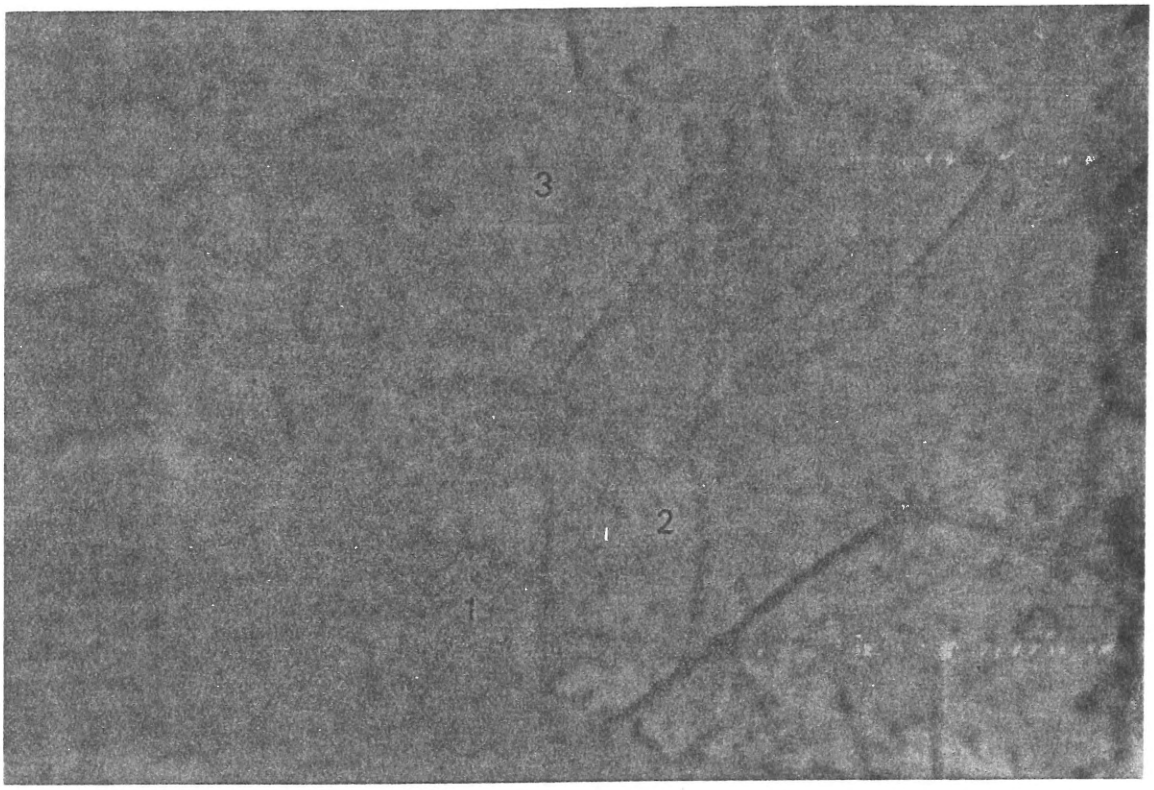

Figure 21C. Sample BH-20-4.1. Reflected light. Pyrrhotite (taupe) with chalcopyrite (dark gold) (f.o.v. 5.75 mm).

Location		1	2	3
Atomic %	**Fe**	25.142	46.734	46.459
	S	49.622	53.266	53.159
	Cu	25.087	0	0
Total		99.851	100.00	99.618
Element %	**Fe**	30.477	60.316	56.783
	S	34.530	39.463	37.296
	Cu	34.598	0	0
Total		99.606	99.779	94.079
Mineral Name		chalcopyrite	pyrrhotite	pyrrhotite

Figure 22C. Sample BH-20-4.1. Reflected light. Pyrrhotite (taupe) with pyrite inclusion (white/gold) (f.o.v. 5.75 mm).

Location		1	2	3
Atomic %	Fe	33.458	46.627	46.778
	S	66.165	53.057	53.102
	As	0.165	0.152	0
Total		100.00	99.836	99.880
Element %	Fe	46.673	59.992	60.068
	S	53.151	39.187	39.142
	As	0.309	0.263	0
Total		100.133	99.441	99.210
Mineral Name		pyrite	pyrrhotite	pyrrhotite

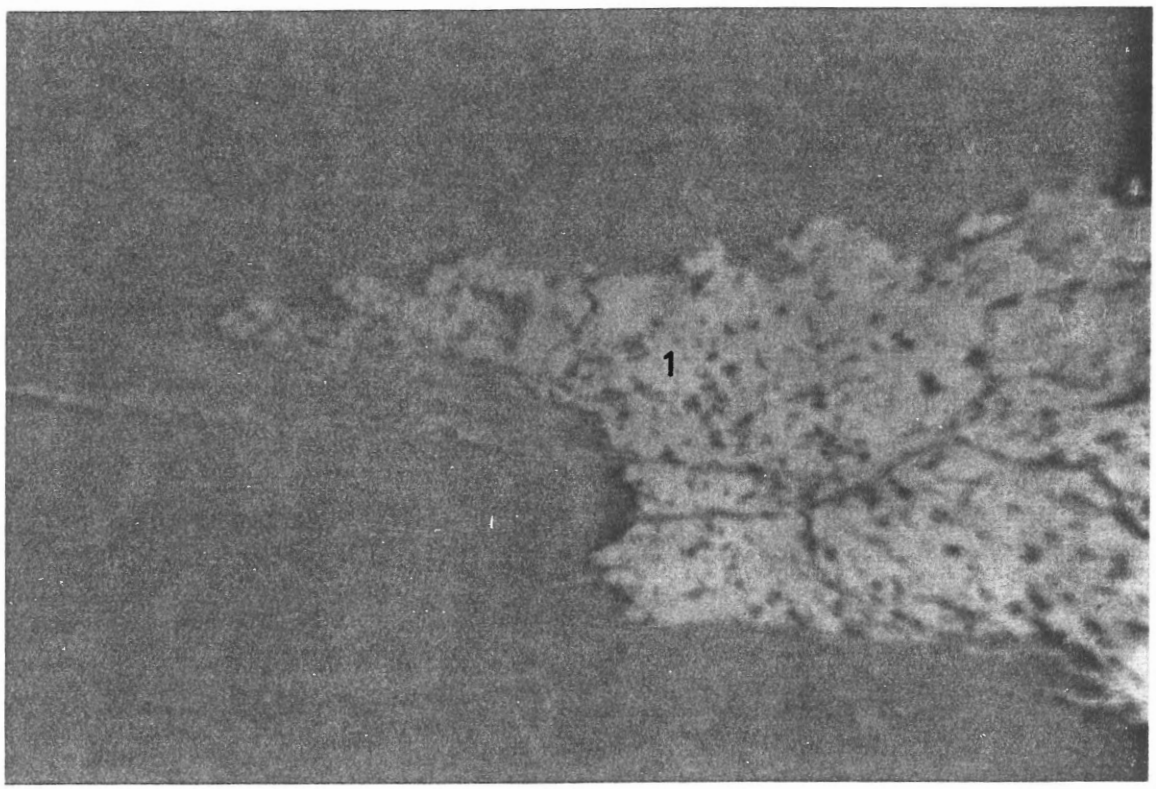

Figure 23C. **Sample BH-20-4.2.** Reflected light. Pyrite (white/gold) with ribboned texture (f.o.v. 5.75 mm).

Location		1
Atomic %	Fe	33.636
	S	66.232
	As	0.133
Total		100.00
Element %	Fe	47.080
	S	53.216
	As	0.249
Total		100.545
Mineral Name		pyrite